第44卷 第3期 岩 石 矿 物 学 杂 志 Vol. 44, No. 3: 501~521
2025年5月 ACTA PETROLOGICA ET MINERALOGICA May, 2025

·专题研究·

Doi: 10.20086/j.cnki.yskw.2025.4108

四川盐源小高山晚二叠世玄武岩矿物学、年代学、地球化学特征及源区和成因意义

李宏博[1,2],章西焕[1],杨小男[1],彭艳菊[1],李常权[2]

(1. 中国地质博物馆,地质标本研究与检测实验室,北京 100034; 2. 中国地质大学地质过程与矿产资源国家重点实验室,北京 100083)

摘 要: 高钛/低钛玄武岩的源区特征和成因机制是大火成岩省研究的重要科学问题,峨眉山大火成岩省亦是如此。本文针对四川盐源小高山晚二叠世玄武岩开展了矿物学、年代学、地球化学和同位素特征研究,结果表明小高山玄武岩属于钠质拉斑玄武岩系列。单斜辉石的结晶温度为1 061~1 180℃,压力为190~352 MPa。Fe-Ti氧化物的X_{Mt}值(0.24~0.38)指示了较低的氧逸度,有利于向Fenner趋势演化。LA-ICP-MS锆石U-Pb年代学分析结果表明小高山晚二叠世玄武岩的结晶年龄为260.2±5.0 Ma,是峨眉山溢流玄武岩喷发峰期的产物。稀土和微量元素模式图与洋岛玄武岩(OIB)相似,并呈现向E-MORB过渡的趋势。$(^{87}Sr/^{86}Sr)_i$=0.704 650~0.705 035, $\varepsilon Nd(t)$=+2.91~+3.02。地球化学和同位素特征表明小高山晚二叠世玄武岩未遭受明显地壳混染,源区以地幔柱组分为主,与平川铁矿苦橄斑岩具有同源性,是连续演化的产物。REEBOX PRO模拟表明,峨眉山玄武岩的源区组分具有原始地幔特征。当岩石圈较厚(140 km)时,只能产生高钛玄武岩(t_p=1 550~1 690℃)。岩石圈大幅减薄之后(50 km),扩大的熔融区间(t_p=1 400~1 690℃)既可以熔出高钛玄武岩,也可产生低钛玄武岩。因此,峨眉山低钛/高钛玄武岩可由同一地幔源区经过连续熔融产生。模拟还表明小高山玄武岩形成于较薄岩石圈条件,形成的温压范围是1 403℃/2.38×10^3 MPa~1 557℃/3.55×10^3 MPa。

关键词: 地球化学; Sr-Nd同位素; REEBOX PRO模拟; 峨眉山大火成岩省; 地幔柱; 四川盐源小高山

中图分类号: P588.14+5; P597 **文献标识码**: A **文章编号**: 1000-6524(2025)03-0501-21

Mineralogical, geochronological, geochemical characteristics and petrogenesis significances of the Late Permian basalts in Xiaogaoshan, Yanyuan, Sichuan

LI Hong-bo[1,2], ZHANG Xi-huan[1], YANG Xiao-nan[1], PENG Yan-ju[1] and LI Chang-quan[2]

(1. Laboratory of Geo-specimens Study and Testing, The Geological Museum of China, Beijing 100034, China; 2. State Key Laboratory of Geological Processes and Mineral Resources, China University of Geosciences, Beijing 100083, China)

Abstract: The source characteristics and origin of high-Ti (HT) and low-Ti (LT) magma types are the first-order geodynamic question for the Large Igneous Provinces (LIPs) and mantle plume, especially the Emeishan LIP (ELIP). In this study, we report LA-ICP-MS zircon U-Pb ages, as well as mineralogical, geochemical, and Sr-Nd isotopic data on the Late Permian basalts in the Xiaogaoshan, Yanyuan, Sichuan. The Xiaogaoshan basalts can be classified as LT/HT transitional type and sodic tholeiitic rock series. Clinopyroxene crystallization temperature and pressure are 1 061 to 1 180℃ and 190 to 352 MPa. The X_{Mt} of Fe-Ti oxides (0.24 to 0.38) indicates a relatively low oxygen fugacity environment and the Fenner trend of fractional crystallization (evolving to iron-enriched). The zircon U-Pb data yield age is 260.2±5.0 Ma, *i.e.*, the peak magmatism of the ELIP. The chondrite-normal-

收稿日期: 2024-05-19; **接受日期**: 2025-01-15; **编辑**: 尹淑苹

基金项目: 自然资源部部门预算项目(12111300000018001-02); 国家自然科学基金项目(41772057)

作者简介: 李宏博(1978-),男,博士,正高级工程师,从事岩浆岩岩石学、地球化学研究工作,E-mail: li_h_b@sina.com.cn。

ized rare earth elements (REE) patterns and the primitive mantle-normalized spidergrams show oceanic island basalt (OIB) affinity, with a trend to E-MORB (enriched Mid-Ocean Ridge Basalts). The rocks have low age-corrected ($^{87}Sr/^{86}Sr)_i$ ratios (0.704 650 to 0.705 035) and positive $\varepsilon Nd(t)$ values (+2.91 to +3.02). The geochemical and isotopic features suggest that the lavas have not undergone any significant crustal contamination, and the source is dominated by "plume" components. The Late Permian Xiaogaoshan basalts have a co-genetic relationship with the picritic porphyries in the Pingchuan iron oxide deposit via fractional crystallization. REEBOX PRO modeling of the adiabatic decompression melting for the Emeishan basalts indicate that the mantle sources of the Emeishan basalts are characterized by the primitive mantle (PM). Only HT basalts can be generated at elevated mantle potential temperatures (t_p = 1 550℃ to 1 690℃) beneath a lithosphere that is 140 km thick. In contrast, expanded melting temperatures (t_p = 1 400℃ to 1 690℃) and regime spread over LT and HT basalts beneath a considerably thinned lithosphere (50 km). Therefore, the origin of the Emeishan basalts, both LT and HT, is through a continuous melting process of the same source. The modelling suggests that the Xiaogaoshan basalts most likely formed under a thinner lithosphere (50 km), with melting temperature and pressure conditions of 1 403℃/2.38×10^3 MPa to 1 557℃/3.55×10^3 MPa.

Key words: geochemistry; Sr-Nd isotope; REEBOX PRO modeling; Emeishan Large Igneous Province; mantle plume; Xiaogaoshan, Yanyuan, Sichuan

Fund support: Department Budget Project, Ministry of Natural Resources of PRC (121113000000018001-02); National Nature Science Foundation of China (41772057)

大火成岩省(Large Igneous Provinces, LIPs)是地球演化历史中的重大地质事件,以短时间内的巨量熔岩喷发为特征(Bryan and Ernst, 2008),目前普遍认为 LIPs 的形成与地幔柱作用有关(Campbell and Griffiths, 1990; Hill, 1991; Saunders, 2005)。大陆溢流玄武岩往往被划分为低钛和高钛两种类型,比如:Siberian、Paraná-Etendeka、Karoo、Emeishan(Lightfoot *et al.*, 1993; Ewart *et al.*, 2004; Xiao *et al.*, 2003, 2004; Jourdan *et al.*, 2007)。高钛型一般被解释为深部源区通过较低程度部分熔融产生的熔体,而低钛型则被认为是在浅部经较大程度部分熔融的产物(Tegner *et al.*, 1998; Jourdan *et al.*, 2007; Marzoli *et al.*, 2019)。然而,某些高钛和低钛玄武岩的地球化学特征存在较大程度的重叠(Hou *et al.*, 2011; Luttinen, 2018),导致对岩浆源区和成因存在不同程度的争议。

峨眉山大火成岩省(Emeishan LIP, ELIP)的情况也是如此。依据 TiO_2 含量以及 Ti/Y 值,峨眉山玄武岩被划分为高钛(HT)和低钛(LT)两种类型(Xu *et al.*, 2001)。此外,张招崇等(2001)根据 Ti 和 P 之间的正相关性提出了另一种划分方案,即高 P 高 Ti 型(HPT)和低 P 低 Ti 型(LPT)。Xu 等(2001)将高钛型(HT)进一步划分为 HT1 型、HT2 型和 HT3 型,Xiao 等(2004)则将低钛型(LT)进一步划分为 LT1 型和 LT2 型。然而,关于峨眉山高钛/HPT 和低钛/LPT 玄武岩的源区和成因机制问题依然存在争议,学者们提出了不同的模型,比如,低钛地幔柱起源(姜常义等, 2007; Xu *et al.*, 2007);低钛 SCLM(subcontinental lithospheric mantle)起源(Tian *et al.*, 2017; Huang *et al.*, 2022a);高钛地幔柱起源(Tian *et al.*, 2017; Li *et al.*, 2017a);高钛 SCLM 起源(Lai *et al.*, 2012; Zhou *et al.*, 2006)。也有学者提出高钛/HPT 和低钛/LPT 的源区组分并非单一组分,而是地幔柱与岩石圈地幔不同程度混合的产物(Chung and Jahn, 1995; Xiao *et al.*, 2003, 2004)。

然而,由于峨眉山玄武岩的 TiO_2 含量变化具有连续性(1%~5%),高钛(HT)和低钛(LT)的划分方案遭受了一些质疑。一些学者提出峨眉山玄武岩不同的 TiO_2 含量是同源岩浆(苦橄-玄武质岩浆)经过不同矿物相的分离结晶作用而导致的,其中 Fe-Ti 氧化物的分离结晶是 TiO_2 含量以及 Ti/Y 值的关键控制因素(张招崇等, 2001; 郝艳丽等, 2004; 张招崇, 2009; 董书云等, 2009; Hou *et al.*, 2011)。也有学者强调低钛/高钛玄武岩具有相同的源区,而熔融压力和部分熔融程度是决定性因素,并提出了一个连续变压熔融模型(Shellnutt and Jahn, 2011; Ren *et al.*, 2017; Zhang *et al.*, 2019)。

四川盐源小高山地区位于 ELIP 内带，峨眉山玄武岩十分发育（Liu *et al.*，2015；张磊等，2022；图 1a）。本文对区内发育的玄武岩开展了锆石 U-Pb 测年、电子探针、主微量元素、Sr-Nd 同位素的系统研究，查明了其矿物学、岩石学、年代学、地球化学以及同位素特征。在此基础上采用 REEBOX PRO（v. 1. 1）对峨眉山玄武岩的熔融过程进行正向模拟，探究峨眉山玄武岩的源区特征以及成因机制。

1　地质背景

1.1　峨眉山大火成岩省

峨眉山大火成岩省（ELIP）分布于中国西南地区以及越南北部一带，位于青藏高原东部，扬子克拉通西缘（Chung and Jahn，1995；Xu *et al.*，2001）（图 1a）。ELIP 面积约 $5\times10^5\sim7\times10^5$ km^2，由广布的

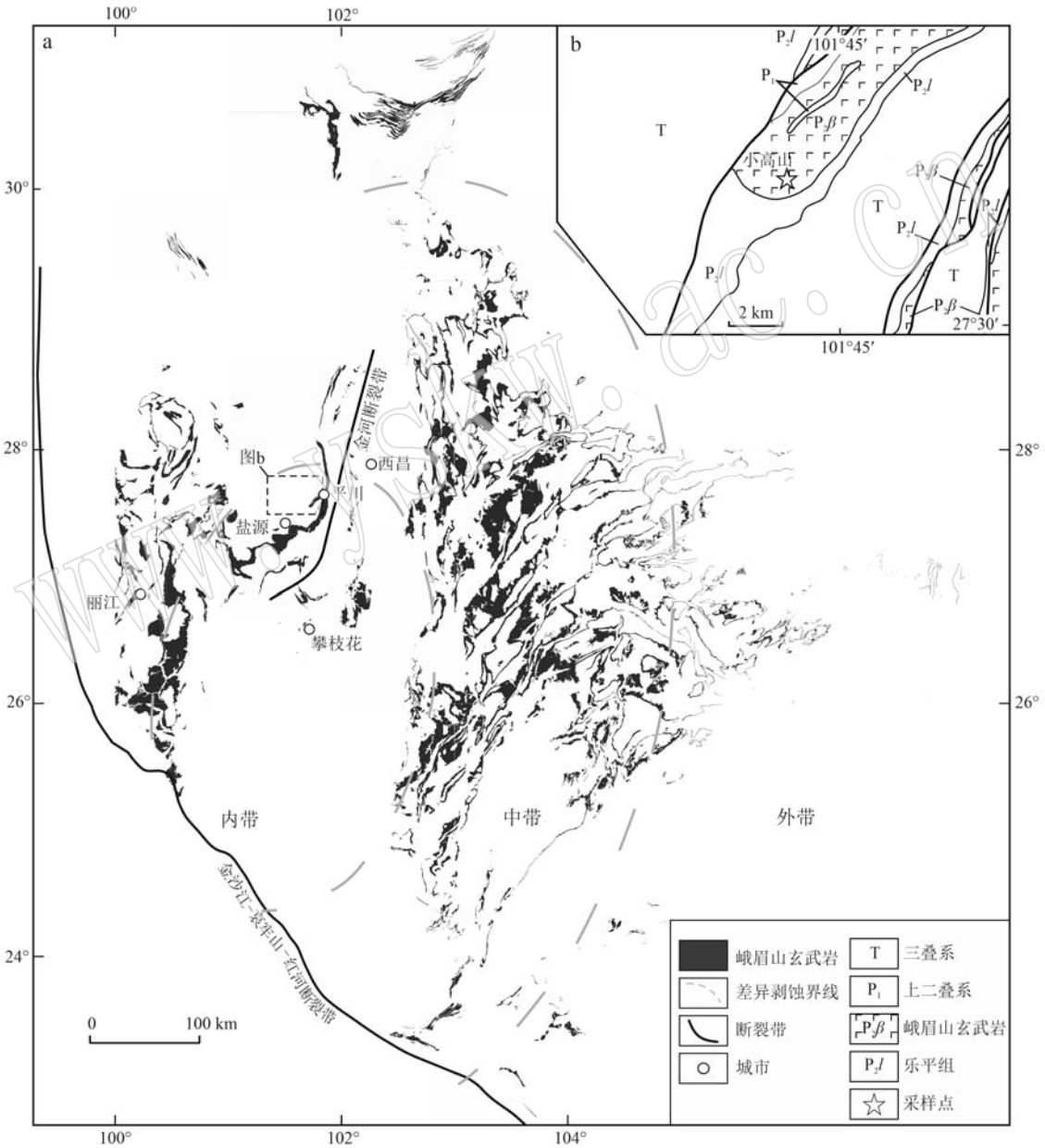

图 1　峨眉山大火成岩省分布图（a，据 Li *et al.*，2017a 修改，其中差异剥蚀界线据 He *et al.*，2003）和四川盐源小高山地质简图（b，据四川地质局第 1 区测队，1971）

Fig. 1　Distribution map of the Emeishan Large Igneous Province (a, modified from Li *et al.*, 2017a, and boundaries of differential erosion zones are from He *et al.*, 2003) and Geological sketch map of the Xiaogaoshan, Yanyuan, Sichuan (b, after Regional Geological Survey Team No. 1, Sichuan Geological Bureau, 1971)

大陆溢流玄武质熔岩(包括少量苦橄岩、安山质玄武岩),以及同期的超基性-基性-酸性侵入岩体组成,普遍认为是一次地幔柱作用的产物(Xu *et al.*, 2001; Xiao *et al.*, 2004; Zhang *et al.*, 2006; Zhou *et al.*, 2006; Li *et al.*, 2015, 2017a)。熔岩厚度呈西厚(>5 000 m)东薄(仅几百米)的变化趋势(Xiao *et al.*, 2004; Zhang *et al.*, 2006)。峨眉山玄武岩与下伏中二叠统茅口组灰岩呈喷发不整合接触,与上覆的上二叠统呈不整合/整合接触关系(Chung and Jahn, 1995; Xiao *et al.*, 2004)。根据茅口组灰岩遭受的差异剥蚀情况,He 等(2003)将 ELIP 由内至外划分为3个区域,即内带、中带和外带(图1a)。同位素年代学和生物地层学研究,特别是近年的一些高精度同位素定年结果表明,峨眉山玄武岩是在较短时间内喷发完成的(260~257 Ma),其喷发峰期在260 Ma左右(He *et al.*, 2007; Sun *et al.*, 2010; Li *et al.*, 2016; Zhong *et al.*, 2020; Huang *et al.*, 2022b)。ELIP 赋存着丰富矿产资源,其中攀西地区(攀枝花-西昌)发育的众多镁铁-超镁铁质层状岩体孕育了全球最大的钒钛磁铁矿矿集区(Zhang *et al.*, 2009; 王焰等, 2017)。

1.2 盐源小高山地质特征及玄武岩岩相学特征

小高山地区位于古生代台地边缘沉降带,地处盐源-丽江台缘坳陷带的东缘与康滇地轴中段西缘的结合部(郭孟明, 1990)。小高山地区与攀西地区具有相同的前寒武基底,上覆地层由古生界地层(奥陶系到二叠系)和三叠系地层组成。二叠系地层包括下二叠统(P_1,茅口组、栖霞组、梁山组,灰岩、泥灰岩、砂岩、泥岩)、上二叠统峨眉山玄武岩($P_2\beta$)以及上二叠统乐平组(P_2l, 砂岩、粉砂岩、炭质页岩)。其中,峨眉山玄武岩主要出露于金河断裂带西盘,呈南北向弧形展布(图1b)。峨眉山玄武岩与下伏的下二叠统以及上覆的上二叠统乐平组均为假整合接触关系。区内平川铁矿紧邻攀西矿集区,其形成与 ELIP 的岩浆作用密切相关(Wang *et al.*, 2014; Liu *et al.*, 2015)。

小高山晚二叠世玄武岩呈铁灰色、灰绿色(图2a),具典型的间粒结构(图2b)、斑状结构(图2c),致密块状构造、杏仁状构造(图2d)。斑晶为斜长石、辉石,粒径大小不一(图2b和2d)。斜长石为自形-半自形长板状,粒径一般为0.1~0.3 mm,也可见粒径达2.5 mm的大斑晶(图2d),含量35%~45%。辉石为半自形至他形,偶见自形晶,粒径0.05~0.34 mm,含量15%~25%。Fe-Ti 氧化物多为他形,散布于基质中,含量~5%。岩石蚀变程度不一,主要是钠长石化、绿泥石化。

2 测试方法

锆石分选工作在河北省地质测绘院实验室完成。北京中兴美科科技有限公司完成锆石制靶、显微(反射光和透射光)及阴极发光(CL)照相。测试前仔细观察锆石晶形与内部结构特征,选择环带清晰、晶形完好的锆石,避开裂隙、包体进行测试选点。相关制靶和实验流程参见宋彪等(2002)。LA-ICP-MS 锆石 U-Pb 法测年在中国地质科学院地质研究所大陆构造与动力学实验室完成。测年采用的 MC-ICP-MS 为 Neptune Plus 型多接收等离子体质谱仪。激光剥蚀以氦气作为剥蚀物质的载气,激光剥蚀束斑直径为32 μm,激光能量密度为10 J/cm^2,频率为8 Hz。每个分析点的气体背景采集时间为4 s,信号采集时间为23 s。数据分析前,采用国际通用的锆石标样91500作为参考物质进行仪器的最佳化。选用 GJ-1 作为辅助标样对数据的准确性进行验证。

电子探针测试在中国地质大学(北京)电子探针室完成。仪器型号为日本岛津 EPMA-1600 型电子探针仪,测试电压为15 kV,电流为1×10^{-7} mA,束斑为1 μm。根据电子探针国标,主量元素测试允许的相对误差≤5%。标准样品为美国 SPI 公司研制的电子探针标准物质,包括 Si、Al、Na(长石)、Ti(金红石)、Fe(铁铝榴石)、Mn(蔷薇辉石)、Ca(方解石)、K(透长石)、Rb(铯榴石)。

主量元素和微量元素(包括稀土元素)分析在国家地质实验测试中心完成。首先,新鲜岩石样品破碎至厘米大小,然后用去离子水清洗并干燥,再粉碎至200目以下。采用X荧光光谱仪分析主量元素,使用标准样品 GSR1、GSR8、GSR9 和 GSR15 进行监测校准。采用 ELEMENTXR 等离子体质谱仪分析微量元素,采用国家标准样品 GSR1、GSR2 和 GSR4 进行监测校准。测试精度为:Fe_2O_3 和 FeO 的 RSD<10%,其他主量元素的 RSD<8%,微量和稀土元素的 RSD<10%。

Sm-Nd、Rb-Sr 元素含量以及同位素比值测定在南京大学现代分析中心完成,分析仪器为英国制造的 VG354 多接收质谱计。样品在80℃下用混合酸溶解(盐酸和硝酸比例为1∶3),取清液上离子交换

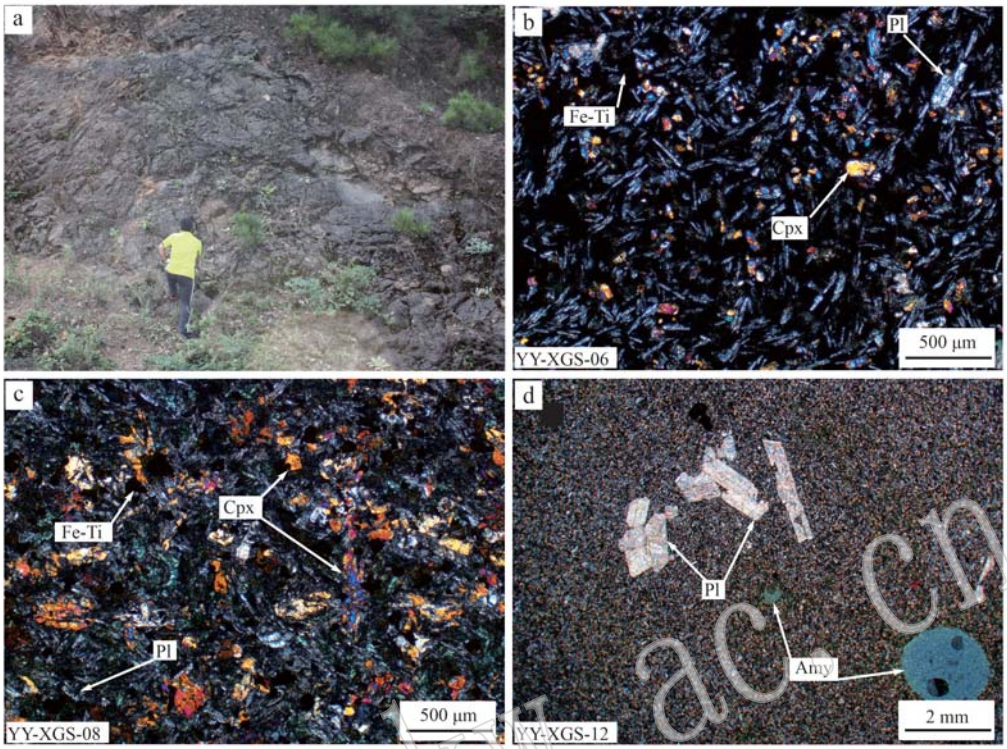

图 2　四川盐源小高山晚二叠世玄武岩野外(a)及显微镜下照片(b、c、d,正交偏光)

Fig. 2　Field photograph (a) and microphotographs (b, c, d, cross-polarized light) of the Xiaogaoshan basalts, Yanyuan, Sichuan

a—野外玄武质熔岩层; b—间粒结构,自形-半自形的长板状斜长石晶粒杂乱排布,细小的他形单斜辉石充填空隙; c—斑状结构,粒径较大的单斜辉石斑晶,呈半自形-他形; d—斜长石大斑晶分布于基质之中,钠长石化,杏仁构造; Cpx—单斜辉石; Pl—斜长石; Fe-Ti—铁钛氧化物; Amy—杏仁构造

a—the Late Permian basaltic lava at field; b—intergranular texture, euhedral-subhedral, plagioclase laths with interstitial xenomorphic, fine clinopyroxene and Fe-Ti oxides; c—porphyritic texture, subhedral-xenomorphic, coarse-grained clinopyroxene phenocryst; d—large euhedral plagioclase phenocryst, albitization, amygdaloidal structure; Cpx—clinopyroxene; Pl—plagioclase; Fe-Ti—Fe-Ti oxides; Amy—amygdaloidal structure

柱分离,采用高压密闭熔样和阳离子交换技术分离和提纯,测定方法参见 Wang 等(2007b)。实验校正采用 Sr 同位素标准样 NBS 987,$^{86}Sr/^{88}Sr = 0.1194$ 为标准化值,测得 $^{87}Sr/^{86}Sr = 0.710\ 224 \pm 8$ ($n = 10$);Nd 同位素标准样为 La Jolla, $^{146}Nd/^{144}Nd = 0.721\ 9$ 为标准化值,测得 $^{143}Nd/^{144}Nd = 0.511\ 860 \pm 8$ (2σ, $n = 8$)。Nd 和 Sr 的全流程本底分别为 6×10^{-11} g 和 3×10^{-9} g。计算 $\varepsilon Nd(t)$ 和 $\varepsilon Sr(t)$ 过程中,$(^{143}Nd/^{144}Nd)_{CHUR} = 0.512\ 638$, $(^{147}Sm/^{144}Nd)_{CHUR} = 0.196\ 7$; $(^{87}Sr/^{86}Sr)_{UR} = 0.704\ 5$; $(^{87}Rb/^{86}Sr)_{UR} = 0.082\ 7$。

3　分析结果

3.1　电子探针

小高山玄武岩代表性长石、辉石以及 Fe-Ti 氧化物的电子探针分析结果列于表 1 至表 3。小高山玄武岩的斜长石成分范围有一定变化,主要是拉长石和中长石($Ab_{40\sim62}An_{34\sim59}Or_{1\sim10}$),部分长石发生钠长石化蚀变(表 1;图 3b)。辉石为普通辉石($Wo_{36\sim44}En_{33\sim49}Fs_{11\sim21}$;图 3a),$Al_2O_3$ 含量为 2.22%~5.50%,TiO_2 含量为 0.54%~2.87%,Na_2O 含量为 0.27%~0.67%,$Mg^{\#}$ 值为 62~82。根据单斜辉石温压计(Wang *et al.*, 2021),计算出单斜辉石的结晶温度为 1 061~1 180℃,压力为 190~352 MPa(表 2)。小高山玄武岩的 Fe-Ti 氧化物成分变化较大,既有磁铁矿(TiO_2 = 1.38%~9.09%, FeO = 80.73%~88.11%)、含钛磁铁矿(TiO_2 = 16.46%~22.39%, FeO = 66.29%~69.23%),又有钛铁矿(TiO_2 = 47.95%~48.71%, FeO = 43.49%~44.91%)(表 3)。

3.2　LA-ICP-MS 锆石 U-Pb 年龄

小高山玄武岩锆石颗粒是透明的、自形至半自形,呈短柱状,粒径为 56~100 μm,长宽比为 1.1~2.5(图4a)。锆石颗粒具有较高的Th含量(76×10^{-6}~

表 1 小高山玄武岩长石电子探针分析结果 w_B/%

Table 1 Microprobe analyses of the feldspar in the Xiaogaoshan basalt

分析点号	pl01	pl02	pl03	pl04	pl05	pl06	pl07	pl08	pl09	pl10	pl11	pl12
长石类型	斜长石	斜长石	斜长石	斜长石	斜长石	斜长石	斜长石	斜长石	斜长石	斜长石	钠长石	钠长石
SiO_2	51.84	51.36	51.70	54.17	56.75	52.58	54.43	53.81	54.39	55.59	65.07	66.14
TiO_2	0.38	0.11	0.18	0.00	0.15	0.35	2.10	0.16	0.13	0.17	0.09	0.04
Al_2O_3	29.28	28.99	29.13	27.70	25.80	28.35	25.65	27.30	26.48	27.12	20.03	19.86
FeO	0.88	1.07	1.16	0.91	1.11	0.82	1.70	1.08	1.28	0.86	0.28	0.04
MnO	0.07	0.31	0.12	0.00	0.00	0.08	0.00	0.00	0.15	0.00	0.14	0.00
MgO	0.20	0.05	0.16	0.06	0.09	0.14	0.58	0.02	0.00	0.08	0.11	0.00
CaO	12.15	12.32	11.99	10.63	7.76	11.30	7.57	10.05	9.03	9.53	1.39	0.74
Na_2O	5.10	4.63	4.97	5.97	7.78	5.44	5.73	6.02	6.84	6.01	12.64	12.82
K_2O	0.20	0.18	0.29	0.25	0.72	0.51	1.70	0.60	0.62	0.69	0.00	0.02
Cr_2O_3	0.00	0.01	0.00	0.07	0.00	0.00	0.10	0.03	0.04	0.00	0.13	0.00
CoO	0.00	0.00	0.08	0.08	0.00	0.08	0.00	0.00	0.00	0.00	0.02	0.00
NiO	0.00	0.27	0.03	0.01	0.00	0.32	0.00	0.09	0.00	0.00	0.00	0.00
总计	100.10	99.29	99.79	99.85	100.16	99.95	99.56	99.16	98.95	100.05	99.89	99.66
以8个氧离子和5个阳离子为基准												
Si	2.389 9	2.392 1	2.394 3	2.481 4	2.587 9	2.431 7	2.577 2	2.490 0	2.525 4	2.532 6	2.903 5	2.929 4
Al	1.590 9	1.591 1	1.589 8	1.495 4	1.386 6	1.545 5	1.431 4	1.489 2	1.449 1	1.456 2	1.053 2	1.036 6
Ca	0.600 1	0.614 6	0.594 9	0.521 7	0.379 3	0.559 8	0.384 0	0.498 3	0.449 3	0.465 2	0.066 3	0.035 3
Na	0.455 9	0.418 4	0.446 3	0.530 2	0.688 0	0.487 4	0.526 0	0.540 1	0.615 7	0.530 9	1.093 7	1.101 0
K	0.011 8	0.010 6	0.017 0	0.014 6	0.042 1	0.029 8	0.102 7	0.035 7	0.036 8	0.040 1	0.000 0	0.001 1
总计	5.048 6	5.026 8	5.042 3	5.043 3	5.083 9	5.054 2	5.021 3	5.053 3	5.076 3	5.025 0	5.116 7	5.103 4
An	56.21	58.90	56.22	48.92	34.19	51.98	37.92	46.39	40.78	44.90	5.71	3.10
Ab	42.69	40.09	42.18	49.71	62.02	45.26	51.94	50.29	55.88	51.23	94.29	96.80
Or	1.10	1.01	1.60	1.37	3.79	2.77	10.14	3.32	3.34	3.87	0.00	0.10

875×10^{-6},平均 300×10^{-6})和 U 含量(75×10^{-6}~324×10^{-6},平均 166×10^{-6}),Th/U 值为 1.01~2.88,平均 1.64,表明锆石为岩浆起源(Belousova *et al.*, 2002;表4)。13 个数据点的 LA-ICP-MS 锆石 U-Pb 测年获得了一个加权平均$^{206}Pb/^{238}U$ 年龄为 260.2±5.0 Ma(图 4b),代表了小高山玄武岩的形成年龄。

3.3 主量、微量元素地球化学特征

四川盐源小高山玄武岩样品的主量、微量元素分析结果列于表 5。SiO_2(44.24%~52.83%)、TiO_2(1.88%~2.94%)、Al_2O_3(12.49%~14.66%)、MnO(0.10%~0.29%)和 P_2O_5(0.22%~0.29%)等主量元素含量的变化幅度较小。然而,其他主量元素成分变化则较大,包括^{T}FeO=9.96%~16.22%(^{T}FeO=FeO+0.899 8×Fe_2O_3;Fe_2O_3=3.52%~9.36%,FeO=3.90%~12.74%)、MgO=3.54%~6.86%、CaO=5.93%~12.29%和全碱含量(Na_2O+K_2O)=0.35%~5.04%。$Mg^{\#}$值为 35~42,表明玄武岩经过了较大程度的演化。$^{T}FeO/MgO-SiO_2$ 岩性判别图中(图 5a),数据点投在了拉斑玄武岩系列之中,且具有较高的 Na_2O 含量(3.03%~4.42%,除了 YY-XGS-04 和 YY-XGS-09),因此小高山晚二叠世玄武岩(Ti/Y=427~535)属于钠质拉斑玄武岩系列(曾令高等,2013)。按照峨眉山玄武岩高钛型和低钛型的划分标准(Xu *et al.*, 2001,TiO_2=2.5%,Ti/Y=500),小高山玄武岩(Ti/Y=427~535)属于低钛/高钛过渡型(图 5b,表 5)。

小高山玄武岩的稀土元素总量较低,∑REE=100×10^{-6}~185×10^{-6},轻稀土元素富集,$(La/Yb)_N$=4.72~6.58,但富集程度略低于 OIB(表 5)。MREE/HREE 以及 HREE 内部的分馏不强烈,这表现在$(Tb/Yb)_N$=1.55~1.94 和$(Dy/Yb)_N$=1.30~1.57。Eu 负异常轻微至明显(δEu=0.78~0.99,图 6a)。原始地幔标准化微量元素蛛网图中(图 6b),随着微量元素不相容性的降低,其标准化值随之降低,总体呈右倾曲线。富集大离子亲石元素,高场强元素(Nb、Ta、Ti)未见异常,存在明显至轻微的 K、Sr 负异常。总体来看,无论是稀土元素还是微量元素,小高山玄武岩均表现出与 OIB 的亲缘性,亦有向 E-MORB 过渡的趋势。

表 2　小高山玄武岩辉石电子探针分析结果　　w_B/%

Table 2　Microprobe analyses of the pyroxene in the Xiaogaoshan basalt

分析点号	cpx01	cpx02	cpx03	cpx04	cpx05	cpx06	cpx07	cpx08	cpx09	cpx10
SiO_2	51.24	51.58	50.81	50.81	50.95	49.22	48.76	49.75	51.88	49.52
TiO_2	0.81	0.69	0.75	0.77	1.03	1.27	1.39	1.33	0.99	1.31
Al_2O_3	3.29	2.33	2.72	2.88	3.08	3.25	3.70	3.79	2.60	2.91
Cr_2O_3	0.34	0.26	0.31	0.17	0.18	0.34	0.93	0.86	0.32	0.08
FeO	7.87	7.13	7.13	8.18	7.74	11.17	8.28	8.82	7.91	10.12
MnO	0.21	0.14	0.15	0.28	0.23	0.30	0.29	0.26	0.27	0.40
MgO	15.87	16.61	16.21	17.17	16.07	15.71	16.12	16.85	17.40	15.83
CaO	19.60	19.76	19.60	18.17	19.25	17.65	18.62	18.38	18.65	18.18
Na_2O	0.35	0.36	0.33	0.29	0.42	0.40	0.42	0.39	0.27	0.49
K_2O	0.03	0.01	0.01	0.02	0.00	0.07	0.07	0.00	0.01	0.00
CoO	0.00	0.03	0.00	0.00	0.00	0.03	0.07	0.00	0.29	0.00
NiO	0.01	0.05	0.00	0.04	0.00	0.03	0.21	0.13	0.14	0.02
Total	99.65	98.98	98.06	98.90	99.03	99.44	98.86	100.55	100.71	98.86
$Mg^{\#}$	78.24	80.60	80.21	78.91	78.73	71.49	77.63	77.30	79.69	73.61
以 6 个氧原子和 4 个阳离子为基准										
Si	1.901 4	1.922 3	1.911 3	1.899 3	1.901 5	1.859 0	1.841 6	1.842 5	1.906 9	1.873 3
Al^{IV}	0.098 6	0.077 7	0.088 7	0.100 7	0.098 5	0.141 0	0.158 4	0.157 5	0.093 1	0.126 7
Al^{VI}	0.045 5	0.024 6	0.031 9	0.026 2	0.037 0	0.003 7	0.006 3	0.008 1	0.019 5	0.003 1
Ti	0.022 5	0.019 4	0.021 2	0.021 7	0.028 9	0.036 1	0.039 5	0.037 0	0.027 4	0.037 3
Cr	0.010 1	0.007 7	0.009 2	0.005 0	0.005 3	0.010 2	0.027 8	0.025 1	0.009 2	0.002 4
Fe^{3+}	0.036 2	0.049 6	0.044 5	0.071 7	0.042 9	0.130 1	0.117 9	0.116 3	0.043 5	0.122 6
Fe^{2+}	0.207 2	0.171 7	0.179 0	0.182 5	0.197 8	0.219 0	0.141 0	0.154 4	0.198 7	0.194 3
Mn	0.006 7	0.004 4	0.004 8	0.008 9	0.007 3	0.009 6	0.009 3	0.008 0	0.008 3	0.012 8
Mg	0.877 8	0.922 8	0.909 0	0.956 8	0.894 1	0.884 6	0.907 6	0.930 4	0.953 5	0.892 7
Ca	0.779 1	0.789 0	0.790 0	0.727 8	0.769 8	0.714 3	0.753 5	0.729 4	0.734 4	0.736 9
Na	0.025 0	0.026 0	0.024 1	0.021 0	0.030 4	0.029 3	0.030 8	0.027 9	0.018 9	0.035 9
K	0.001 3	0.000 5	0.000 5	0.001 0	0.000 0	0.003 4	0.003 4	0.000 0	0.000 5	0.000 0
总计	4.011 4	4.015 7	4.014 0	4.022 5	4.013 5	4.040 0	4.037 1	4.036 5	4.013 7	4.038 0
Wo	40.33	40.18	40.48	36.97	39.63	35.95	38.44	37.10	37.52	36.93
En	45.43	47.00	46.59	48.60	46.03	44.52	46.30	47.32	48.72	44.74
Fs	12.95	11.50	11.70	13.36	12.77	18.05	13.68	14.17	12.79	16.52
$p/10^2$ MPa	2.38	1.15	1.38	1.28	2.37	0.44	0.19	0.30	0.36	0.69
t/℃	1 154	1 161	1 158	1 146	1 152	1 116	1 124	1 129	1 142	1 114
分析点号	cpx11	cpx12	cpx13	cpx14	cpx15	cpx16	cpx17	cpx18	cpx19	cpx20
SiO_2	50.53	51.52	46.23	50.42	48.02	47.54	51.84	51.09	48.96	49.08
TiO_2	1.41	1.00	2.87	1.29	2.13	1.86	0.54	1.16	1.42	1.62
Al_2O_3	3.27	2.56	5.50	2.22	4.95	4.54	2.31	2.26	4.23	4.71
Cr_2O_3	0.27	0.00	0.08	0.16	0.08	0.00	0.00	0.00	0.10	0.00
FeO	9.50	9.27	12.26	12.46	11.00	11.83	6.86	11.51	9.70	9.94
MnO	0.46	0.00	0.29	0.49	0.51	0.29	0.09	0.22	0.00	0.40
MgO	16.21	16.84	11.02	13.83	12.95	12.58	17.50	15.23	14.69	14.01
CaO	18.25	18.47	20.73	18.75	19.74	19.38	19.09	18.52	20.23	20.28
Na_2O	0.47	0.41	0.49	0.46	0.67	0.62	0.31	0.37	0.54	0.59
K_2O	0.00	0.08	0.01	0.00	0.00	0.02	0.00	0.01	0.00	0.00
CoO	0.19	0.33	0.03	0.00	0.07	0.33	0.37	0.00	0.21	0.00
NiO	0.26	0.09	0.00	0.05	0.37	0.28	0.00	0.00	0.20	0.00
总计	100.81	100.57	99.64	100.13	100.49	99.27	98.91	100.38	100.28	100.62
$Mg^{\#}$	75.27	76.40	61.58	66.43	67.75	65.47	81.98	70.24	72.97	71.54
以 6 个氧原子和 4 个阳离子为基准										
Si	1.874 0	1.906 2	1.775 6	1.904 0	1.814 1	1.826 4	1.929 1	1.908 1	1.837 6	1.831 9
Al^{IV}	0.126 0	0.093 8	0.224 4	0.096 0	0.186 0	0.173 6	0.070 9	0.091 9	0.162 4	0.168 1
Al^{VI}	0.017 2	0.017 8	0.024 6	0.002 9	0.034 3	0.032 0	0.030 5	0.007 7	0.024 7	0.039 2
Ti	0.039 3	0.027 8	0.082 9	0.036 5	0.060 6	0.053 8	0.015 1	0.032 7	0.040 1	0.045 5
Cr	0.007 8	0.000 0	0.002 4	0.004 9	0.002 5	0.000 0	0.000 0	0.000 0	0.003 0	0.000 0
Fe^{3+}	0.083 7	0.079 7	0.101 9	0.072 8	0.114 9	0.120 7	0.048 6	0.068 5	0.139 2	0.119 9
Fe^{2+}	0.208 8	0.205 3	0.288 6	0.318 5	0.229 2	0.255 6	0.164 0	0.288 9	0.161 7	0.187 1
Mn	0.014 4	0.000 0	0.009 4	0.015 7	0.016 3	0.009 4	0.002 8	0.007 1	0.000 0	0.012 6
Mg	0.896 1	0.928 8	0.631 0	0.778 6	0.729 5	0.720 5	0.970 8	0.847 9	0.821 9	0.779 2
Ca	0.725 1	0.732 3	0.853 1	0.758 6	0.798 9	0.797 7	0.761 2	0.741 2	0.813 5	0.810 9
Na	0.033 7	0.029 3	0.036 5	0.033 6	0.049 3	0.046 2	0.022 4	0.026 6	0.039 3	0.042 8
K	0.000 0	0.003 9	0.000 5	0.000 0	0.000 0	0.001 0	0.000 0	0.000 5	0.000 0	0.000 0
总计	4.026 1	4.024 9	4.030 9	4.022 0	4.035 3	4.036 8	4.015 4	4.020 9	4.043 4	4.037 3
Wo	36.96	37.07	44.42	38.36	41.22	40.91	38.64	37.43	41.18	41.53
En	45.68	47.02	32.86	39.37	37.64	36.95	49.29	42.82	41.60	39.91
Fs	15.64	14.43	20.82	20.58	18.60	19.78	10.94	18.40	15.23	16.37
$p/10^2$ MPa	1.88	1.27	1.01	0.72	3.52	3.09	1.89	0.25	1.43	2.76
t/℃	1 119	1 164	1 061	1 091	1 086	1 100	1 180	1 121	1 136	1 103

表 3 小高山玄武岩 Fe-Ti 氧化物电子探针分析结果 w_B/%

Table 3 Microprobe analyses of Fe-Ti oxides in the Xiaogaoshan basalt

分析点号	mag01	mag02	mag03	mag04	mag05	mag06	mag07	mag08
矿物类型	磁铁矿	磁铁矿	磁铁矿	磁铁矿	磁铁矿	磁铁矿	磁铁矿	含钛磁铁矿
SiO_2	2.67	1.78	2.02	1.24	1.68	1.38	2.91	0.11
TiO_2	5.60	1.38	3.01	9.09	5.29	7.56	3.85	16.46
Al_2O_3	1.22	0.11	0.33	0.81	0.37	0.35	0.30	5.49
FeO	80.73	88.11	84.85	81.57	83.12	80.86	83.67	69.23
MnO	0.34	0.28	0.17	0.01	0.13	0.21	0.05	0.51
MgO	0.00	0.11	0.05	0.01	0.03	0.15	0.03	0.11
CaO	0.76	0.24	0.35	0.24	0.36	0.60	0.82	0.13
Na_2O	0.21	0.37	0.19	0.29	0.30	0.21	0.26	0.15
K_2O	0.08	0.00	0.04	0.07	0.00	0.01	0.00	0.03
Cr_2O_3	0.18	0.16	0.24	0.42	0.41	0.03	0.33	0.43
CoO	0.40	0.07	0.69	0.00	0.34	0.44	0.01	0.32
NiO	0.00	0.49	0.33	0.00	0.06	0.24	0.65	0.4
总计	92.20	93.11	92.27	93.74	92.09	92.04	92.88	93.37
Si	0.103 7	0.068 5	0.078 9	0.047 6	0.065 7	0.054 1	0.112 0	0.004 2
Ti	0.163 6	0.039 9	0.088 5	0.262 7	0.155 6	0.223 1	0.111 5	0.474 4
Al	0.055 8	0.005 0	0.015 2	0.036 7	0.017 0	0.016 2	0.013 6	0.247 9
Fe^{3+}	1.399 3	1.758 8	1.633 3	1.323 8	1.521 1	1.420 5	1.514 5	0.772 4
Fe^{2+}	1.222 0	1.075 8	1.139 6	1.296 4	1.196 8	1.232 3	1.178 9	1.445 8
Mn	0.011 2	0.009 1	0.005 6	0.000 3	0.004 3	0.007 0	0.001 6	0.016 6
Mg	0.000 0	0.006 3	0.002 9	0.000 6	0.001 7	0.008 8	0.001 7	0.006 3
Ca	0.031 6	0.009 9	0.014 7	0.009 9	0.015 1	0.025 2	0.033 8	0.005 3
Na	0.015 8	0.027 6	0.014 4	0.021 6	0.022 7	0.016 0	0.019 4	0.011 1
K	0.004 0	0.000 0	0.002 0	0.003 4	0.000 0	0.000 5	0.000 0	0.001 5
Cr	0.005 5	0.004 9	0.007 4	0.012 8	0.012 7	0.000 9	0.010 0	0.013 0
Ni	0.000 0	0.015 2	0.010 4	0.000 0	0.001 9	0.007 6	0.020 1	0.012 3
总计	3.012 4	3.021 0	3.012 8	3.015 6	3.014 7	3.012 2	3.017 2	3.011 0
X_{Mt}	–	–	–	–	–	–	–	0.38
分析点号	mag09	mag10	mag11	mag12	mag13	mag14	mag15	mag16
矿物类型	含钛磁铁矿	含钛磁铁矿	含钛磁铁矿	含钛磁铁矿	钛铁矿	钛铁矿	钛铁矿	钛铁矿
SiO_2	0.29	0.34	0.35	0.29	1.30	0.20	0.16	0.18
TiO_2	16.64	20.93	17.03	22.39	48.71	47.95	47.96	48.71
Al_2O_3	5.74	3.74	5.67	2.45	0.35	0.25	0.28	0.08
FeO	68.76	67.67	68.02	66.29	43.49	46.42	44.91	44.37
MnO	0.26	0.72	0.39	0.08	4.76	4.37	4.28	4.49
MgO	0.12	0	0	0	0.04	0.03	0.20	0.23
CaO	0.18	0.29	0.19	0.25	1.22	0.64	0.41	0.61
Na_2O	0.05	0.36	0.26	0.03	0.08	0.04	0.11	0.11
K_2O	0	0	0.01	0	0.11	0.00	0.01	0.00
Cr_2O_3	0.16	0	0.27	0.33	0.00	0.10	0.26	0.42
CoO	0.02	0	0.17	0.5	0.51	0.33	0.37	0.05
NiO	0.11	0	0.39	0.16	0.37	0.00	0.22	0.00
总计	92.33	94.05	92.75	92.77	100.94	100.33	99.17	99.26
Si	0.011 2	0.013 0	0.013 5	0.011 4	0.032 3	0.005 0	0.004 1	0.004 5
Ti	0.482 1	0.603 5	0.493 4	0.663 4	0.911 3	0.902 7	0.914 7	0.925 0
Al	0.260 5	0.168 9	0.257 3	0.113 7	0.010 3	0.007 4	0.008 4	0.002 4
Fe^{3+}	0.745 4	0.591 2	0.709 8	0.523 3	0.095 1	0.174 7	0.144 0	0.128 3
Fe^{2+}	1.469 2	1.577 9	1.480 8	1.660 0	0.809 4	0.796 8	0.808 2	0.808 4
Mn	0.008 5	0.023 4	0.012 7	0.002 7	0.100 3	0.092 6	0.091 9	0.096 0
Mg	0.006 9	0.000 0	0.000 0	0.000 0	0.001 5	0.001 1	0.007 6	0.008 7
Ca	0.007 4	0.011 9	0.007 8	0.010 5	0.032 5	0.017 2	0.011 1	0.016 5
Na	0.003 7	0.026 8	0.019 4	0.002 3	0.003 9	0.001 9	0.005 4	0.005 4
K	0.000 0	0.000 0	0.000 5	0.000 0	0.003 5	0.000 0	0.000 3	0.000 0
Cr	0.004 9	0.000 0	0.008 2	0.010 3	0.000 0	0.002 0	0.005 2	0.008 4
Ni	0.003 4	0.000 0	0.012 1	0.005 1	0.007 4	0.000 0	0.004 5	0.000 0
总计	3.003 2	3.016 7	3.015 5	3.002 7	2.007 4	2.001 3	2.005 3	2.003 6
X_{Mt}	0.37	0.28	0.35	0.24	–	–	–	–

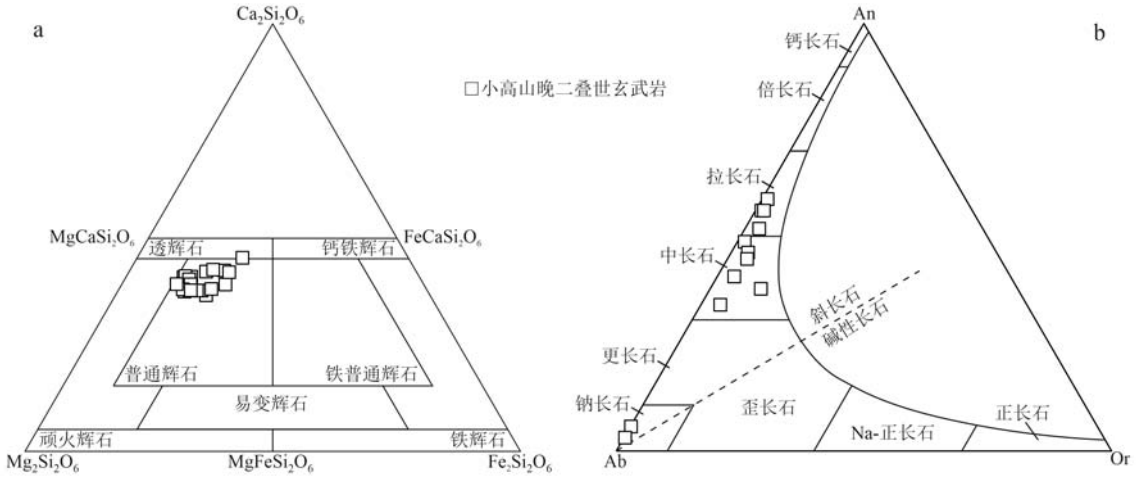

图 3　单斜辉石的硅灰石-顽火辉石-铁辉石分类图解(a，据 Morimoto *et al.*，1988)和长石的钙长石-钠长石-正长石分类图解(b，据 Smith and Brown，1974)

Fig. 3　Wollastonite-enstatite-ferrosilite diagram showing compositions of clinopyroxene (a, after Morimoto *et al.*, 1988) and anorthite-albite-orthoclase diagram showing compositions of feldspars (b, after Smith and Brown, 1974)

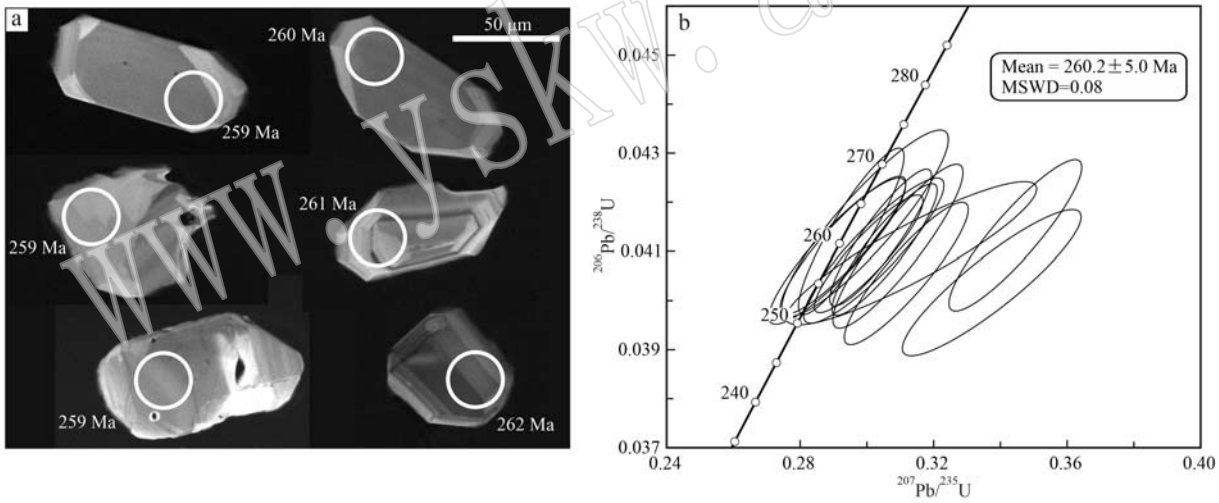

图 4　小高山晚二叠世玄武岩锆石阴极发光图像(a，圆圈为测点位置)和 LA-ICP-MS 锆石年龄谐和图(b)

Fig. 4　CL images of representative zircons from the Xiaogaoshan basalt (a, circles indicate laser points for dating) and LA-ICP-MS U-Pb zircon concordia diagram (b)

3.4　Sr-Nd 同位素

小高山玄武岩的 Sr-Nd 同位素分析结果列于表 6，Sr-Nd 同位素的初始比值均计算至 260 Ma。小高山玄武岩具有较为均一的 Sr-Nd 同位素比值，$(^{87}Sr/^{86}Sr)_i$ 值为 0.704 650～0.705 035，$\varepsilon Nd(t)$ 为 +2.91～+3.02。在 $\varepsilon Nd(t)-(^{87}Sr/^{86}Sr)_i$ 图解中(图 7)，小高山玄武岩的 Sr-Nd 同位素投点都落在 OIB 的范围之内，并与峨眉山苦橄岩重叠(图 7)。

4　讨论

4.1　地壳混染

Nb/U、Nb/Th 是鉴别玄武岩是否受到地壳混染的有效指示剂，比值越低表明遭受地壳混染程度越大(Hofmann，1988)。小高山玄武岩的 Nb/U 和 Nb/Th 值分别为 31～63 和 7.5～9.8，接近大洋玄武

表 4 小高山晚二叠世玄武岩 LA-ICP-MS 锆石 U-Pb 测年分析结果

Table 4 LA-ICP-MS zircon U-Pb analytical results for the Late Permian Xiaogaoshan basalts

分析点号	$w_B/10^{-6}$			Th/U	$^{207}Pb/^{206}Pb\pm1\sigma$	$^{207}Pb/^{235}U\pm1\sigma$	$^{206}Pb/^{238}U\pm1\sigma$	$^{206}Pb/^{238}U$ 年龄$\pm1\sigma$/Ma
	Pb	Th	U					
01	33.40	179.30	125.20	1.43	0.051 8±0.002 2	0.292 9±0.012 4	0.041 1±0.000 9	260±6
02	98.00	543.30	304.90	1.78	0.053 2±0.001 6	0.300 6±0.010 8	0.041 0±0.000 8	259±5
03	22.40	123.50	100.60	1.23	0.051 5±0.002 1	0.291 1±0.013 5	0.041 0±0.001 0	259±6
04	30.30	160.30	101.20	1.58	0.060 6±0.002 8	0.337 4±0.017 7	0.040 4±0.001 0	255±6
05	47.90	255.50	193.60	1.32	0.051 8±0.001 7	0.295 3±0.010 4	0.041 4±0.001 1	262±7
06	26.10	136.10	103.60	1.31	0.054 7±0.002 3	0.309 3±0.012 9	0.041 1±0.001 1	260±7
07	160.00	874.50	323.90	2.70	0.053 5±0.001 8	0.304 2±0.010 1	0.041 3±0.000 9	261±6
08	41.10	200.00	136.90	1.46	0.060 6±0.002 5	0.344 5±0.013 1	0.041 3±0.001 0	261±6
09	36.60	202.70	106.50	1.90	0.055 5±0.004 3	0.313 3±0.024 8	0.041 0±0.001 0	259±6
10	15.30	75.80	75.30	1.01	0.052 4±0.002 7	0.299 5±0.016 5	0.041 6±0.001 3	263±8
11	31.20	170.50	124.10	1.37	0.053 5±0.002 2	0.302 1±0.013 9	0.041 0±0.001 0	259±6
12	121.00	693.30	240.60	2.88	0.055 8±0.001 7	0.311 8±0.012 3	0.040 6±0.001 0	256±6
13	52.80	287.10	215.60	1.33	0.054 0±0.001 6	0.305 3±0.010 4	0.041 0±0.000 9	259±6

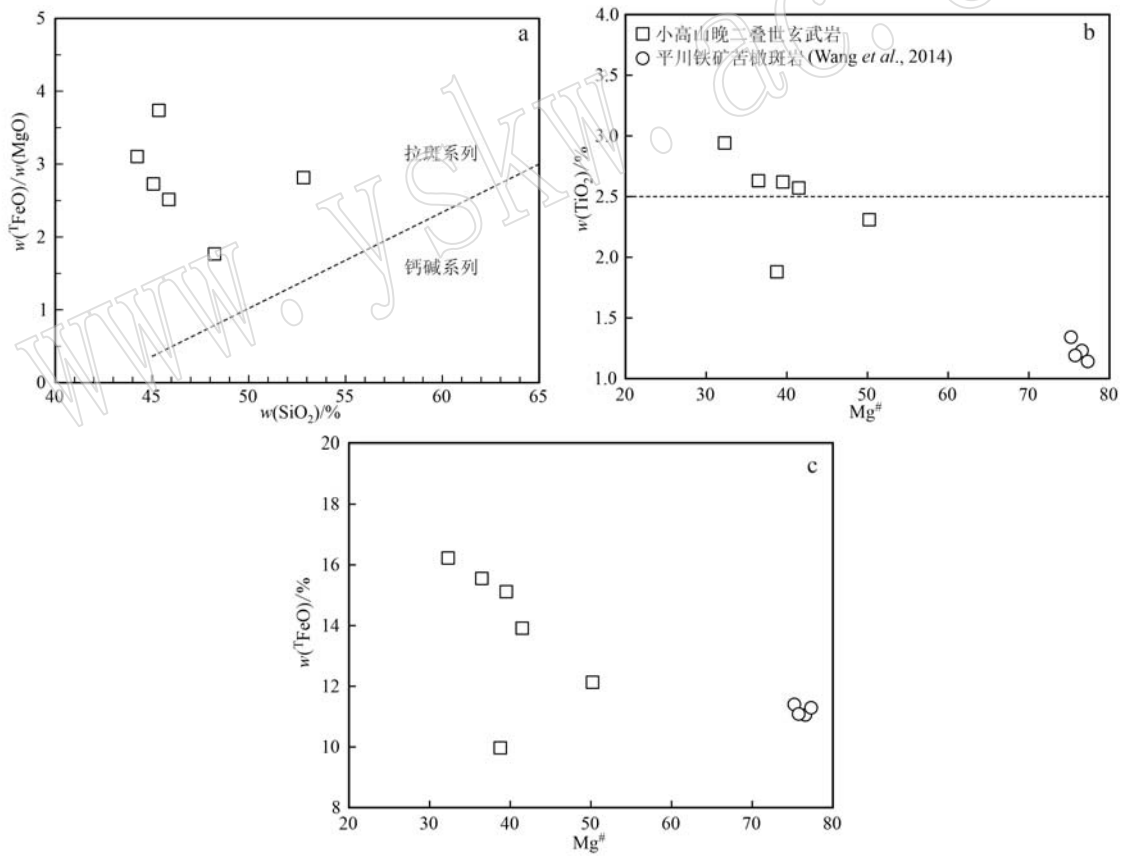

图 5 $^{T}FeO/MgO-SiO_2$ 岩性判别图解(a,据 Miyashiro, 1974)以及哈克图解(b、c)

Fig. 5 $^{T}FeO/MgO-SiO_2$ diagram (a, after Miyashiro, 1974) and Harker diagrams (b and c)

岩(OIB 或 MORB, Nb/U=46~50, Nb/Th=12~19)以及原始地幔(Nb/U = 34, Nb/Th = 8.4, Sun and McDonough, 1989),表明地壳混染不明显。$(Nb/Th)_P-(Th/Yb)_P$ 图解中,小高山玄武岩投点靠近原始地幔和峨眉山苦橄岩,而远离上下地壳,也表明未受到地壳混染的影响(图8a)。同位素方面,相对较低的

表 5　小高山晚二叠世玄武岩全岩主量元素(w_B/%)、微量元素含量(w_B/10^{-6})分析数据表

Table 5　Whole rock analyses of major (w_B/%) and trace elements (w_B/10^{-6}) of the Late Permian Xiaogaoshan basalts

样品 样号	YY-XGS-04	YY-XGS-05	YY-XGS-06	YY-XGS-08	YY-XGS-09	YY-XGS-12
SiO_2	52.83	48.24	44.24	45.08	45.36	45.87
TiO_2	1.88	2.31	2.63	2.62	2.94	2.57
Al_2O_3	12.49	14.56	13.67	14.09	14.66	14.05
Fe_2O_3	6.74	3.52	9.36	6.04	3.87	8.21
FeO	3.90	8.96	7.13	9.68	12.74	6.52
MnO	0.10	0.17	0.23	0.29	0.24	0.23
MgO	3.54	6.86	5.01	5.54	4.34	5.53
CaO	12.29	5.79	9.79	8.84	5.93	9.89
Na_2O	0.31	4.42	3.62	3.50	0.27	3.03
K_2O	0.04	0.62	0.07	0.38	0.29	1.25
P_2O_5	0.23	0.26	0.29	0.29	0.22	0.27
LOI	4.77	3.11	2.54	2.00	6.62	1.24
总计	99.12	98.82	98.58	98.35	97.48	98.66
Rb	1.10	11.0	1.84	8.46	15.7	26.2
Sr	37.6	287	379	602	65.6	404
Ba	14.8	203	144	612	73.8	798
Th	1.47	1.76	2.67	2.70	6.20	2.83
U	0.39	0.39	0.60	0.42	1.42	0.48
Nb	12.1	15.3	24.6	26.5	46.2	26.0
Ta	0.81	1.05	1.60	1.70	2.97	1.67
Zr	168	207	173	180	342	155
Hf	4.61	5.52	4.69	4.81	8.84	4.28
Y	24.0	26.6	34.0	34.5	41.3	28.8
Sc	23.8	28.6	33.8	34.5	33.4	38.0
Co	42.3	54.7	59.7	63.0	75.3	54.3
Ni	75.1	106	54.2	60.8	309	60.7
Cu	41.3	25.4	170	35.6	249	56.4
Pb	3.05	3.64	3.23	3.23	9.06	2.62
Zn	72.7	128	154	211	190	112
V	305	318	477	483	358	454
Cr	57.7	53.0	29.0	40.9	548	59.5
La	14.8	14.8	20.5	21.4	31.9	19.8
Ce	34.2	40.2	44.9	47.8	70.1	43.7
Pr	4.74	5.91	5.96	6.31	9.03	5.77
Nd	21.8	26.9	25.3	26.8	37.0	24.2
Sm	5.35	6.39	5.81	6.15	7.92	5.47
Eu	1.65	1.93	1.97	2.05	2.09	1.85
Gd	5.61	6.75	6.62	6.73	8.42	5.97
Tb	0.89	0.99	1.08	1.12	1.34	0.99
Dy	4.81	5.44	6.15	6.38	7.28	5.49
Ho	0.93	1.01	1.27	1.27	1.42	1.10
Er	2.60	2.90	3.61	3.77	4.09	3.12
Tm	0.32	0.35	0.47	0.50	0.54	0.38
Yb	2.07	2.25	3.08	2.97	3.48	2.63
Lu	0.29	0.31	0.43	0.44	0.50	0.38
∑REE	100	116	127	134	185	121
Ti/Y	469	520	464	455	427	535

放射性 Sr 同位素(0.704 650~0.705 035)以及正的 $\varepsilon Nd(t)$ 值(+2.91~+3.02)印证了以上结论(图 7;表 6)。

4.2　岩浆演化以及对于 Fe 富集的影响

小高山玄武岩具有较低的 $Mg^{\#}$(35~42),表明经过了较大程度的分离结晶。较低的 Ni (54×10^{-6}~106×10^{-6})和 Cr(29.0×10^{-6}~59.5×10^{-6})(表 5,除了 YY-XGS-09)表明可能发生了橄榄石的分离结晶。由于 Eu 和 Sr 对于斜长石均为相容元素,轻微至明显的 Eu 和 Sr 负异常指示了斜长石的分离结晶作用。哈克图解表明,$Mg^{\#}$和 TiO_2、^{T}FeO 呈现明显负相关(图 5b 和 5c),表明岩浆经历了低压环境下的辉石分离结晶。单斜辉石的结晶温压条件计算表明(t=1 061~1 180℃, p=190~352 MPa),小高山玄武岩在上地壳至近地表深度上发生了单斜辉石的分离结晶(表 2)。

低压条件下,拉斑玄武质岩浆有两种分异趋势,一种是较为常见的 Bowen 趋势(贫铁富硅方向演化)(Bowen, 1928; Hunter and Sparks, 1987),另一种是较为少见的 Fenner 趋势(富铁贫硅方向演化)(Fenner, 1929),在大陆溢流玄武岩中更为罕见(Hunter and Sparks, 1987; Brooks *et al.*, 1991; 徐义刚等, 2003)。不同分异趋势主要受磁铁矿分离结晶开始时间的控制,而磁铁矿分离结晶又取决于氧逸度(f_{O_2}, Veklser, 2009)。较高的氧逸度使得岩浆系统中磁铁矿的稳定区间扩大,并导致磁铁矿在早期阶段发生分离结晶(Toplis and Carroll, 1995),而较低的氧逸度则使得熔体中磁铁矿不易达到饱和,从而导致铁的长期富集(Brooks *et al.*, 1991)。Toplis 和 Carroll(1995)指出 Fe-Ti 氧化物的 X_{Mt} 值和岩浆氧逸度(f_{O_2})呈正相关关系。

如前所述,小高山玄武岩具有较高的 ^{T}FeO(12.13%~16.22%,除了 YY-XGS-04),属于铁质玄武岩(表 5;图 5b)。峨眉山大火成岩省东部(比如贵州织金熊家场、水城都格、四川广安阳和;徐义刚等, 2003;廖宝丽等, 2012; Li *et al.*, 2017a)以及中部(比如云南金安地区,汪云峰等, 2013)也发现了类似的情况。小高山玄武岩的 ^{T}FeO 和 TiO_2 随着 $Mg^{\#}$ 降低而增高,而且具有较低的 X_{Mt} 值(0.24~0.38;表 3),并投在了 ELIP 铁质玄武岩区,即 Fenner 趋势(Fenner, 1929;图 8b)。地壳混染会导致岩浆氧逸度(f_{O_2})升高(Juster *et al.*, 1989),然而小高山玄武岩没有遭受明显的地壳混染。以上证据均表明小高山玄武岩形成

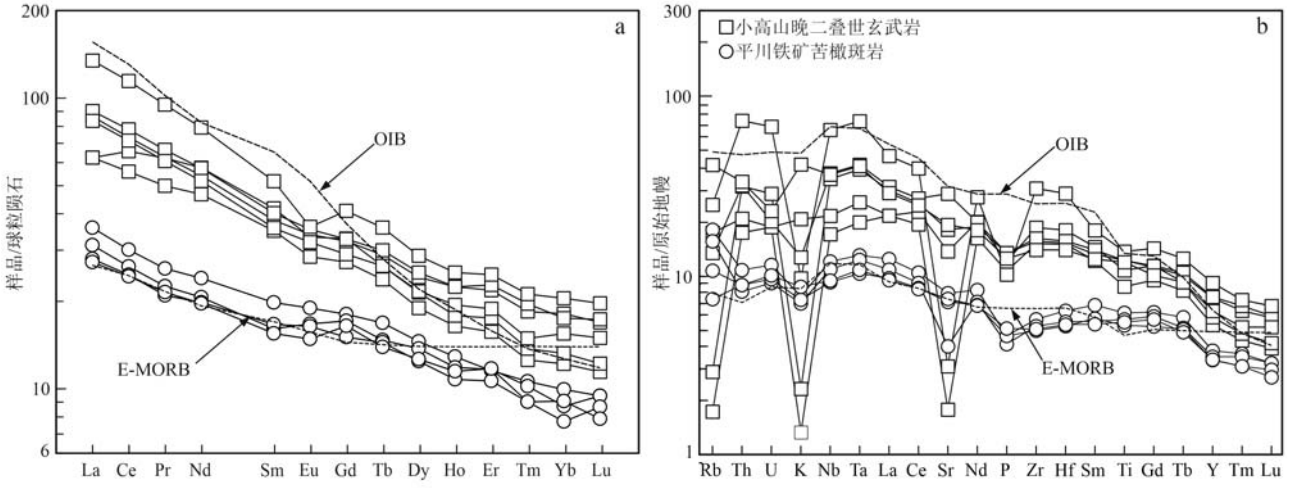

图 6 小高山玄武岩球粒陨石标准化稀土元素配分曲线图(a)和原始地幔标准化微量元素蛛网图(b)

Fig. 6 Bulk chondrite-normalized REE patterns (a) and primitive mantle-normalized trace element spidergrams (b) of the Xiaogaoshan basalt

球粒陨石和原始地幔标准化数据、OIB 以及 E-MORB 引自 Sun and McDonough (1989)

chondrite and primitive mantle values for normalizations, OIB and E-MORB are from Sun and McDonough (1989)

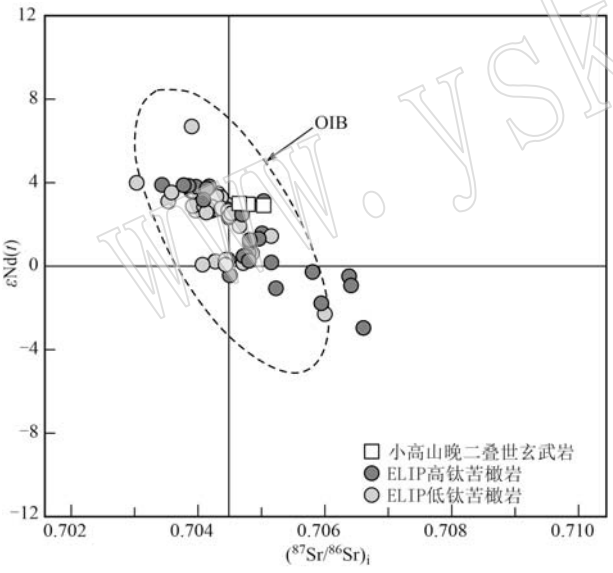

图 7 小高山晚二叠世玄武岩的 $\varepsilon Nd(t)-(^{87}Sr/^{86}Sr)_i$ 图解

Fig. 7 $\varepsilon Nd(t)-(^{87}Sr/^{86}Sr)_i$ plot of the Xiaogaoshan basalt

OIB 数据引自 Lassiter *et al.* (2003), Madureira *et al.* (2011), Hanyu *et al.* (2014)和Garapić *et al.* (2015); ELIP 苦橄岩数据引自 Anh *et al.* (2011), Li *et al.* (2012), Yang and Liu (2019), Zhang *et al.* (2021), Yao *et al.* (2021)和 Yu *et al.* (2024)

data of OIB are from Lassiter *et al.* (2003), Madureira *et al.* (2011), Hanyu *et al.* (2014), and Garapić *et al.* (2015); data of ELIP picrites are from Anh *et al.* (2011), Li *et al.* (2012), Yang and Liu (2019), Zhang *et al.* (2021), Yao *et al.* (2021), and Yu *et al.* (2024)

表 6 小高山晚二叠世玄武岩的 Sr-Nd 同位素分析结果

Table 6 Sr-Nd isotopic data for bulk rocks of the Xiaogaoshan basalt

分析样号	YY-XGS-06	YY-XGS-08	YY-XGS-12
$w(Rb)/10^{-6}$	1.90	8.54	28.01
$w(Sr)/10^{-6}$	382.60	610.80	412.90
$w(Sm)/10^{-6}$	6.03	5.84	5.63
$w(Nd)/10^{-6}$	27.12	24.57	25.39
$^{87}Rb/^{86}Sr$	0.014 8	0.041 6	0.200 7
$^{87}Sr/^{86}Sr$	0.704 704	0.705 189	0.705 531
1σ	0.000 007	0.000 006	0.000 009
$^{147}Sm/^{144}Nd$	0.134 7	0.144 3	0.134 6
$^{143}Nd/^{144}Nd$	0.512 687	0.512 698	0.512 685
1σ	0.000 008	0.000 008	0.000 009
$(^{87}Sr/^{86}Sr)_i$	0.704 650	0.705 035	0.704 789
$(^{143}Nd/^{144}Nd)_i$	0.512 458	0.512 452	0.512 456
$\varepsilon Nd(t)$	3.02	2.91	2.98

于贫水、相对较低氧逸度的还原环境。这种环境有利于单斜辉石(普通辉石)和斜长石的分离结晶,而抑制 Fe-Ti 氧化物的分离结晶(Zhang *et al.*, 2012)。这与岩相学观察吻合,即大量的单斜辉石、斜长石斑晶是早期结晶的,而分布于基质中的细粒、他形 Fe-Ti 氧化物则是晚期结晶的(图 2b 和 2c)。总之,小高山玄武岩的 Fenner 演化趋势(富铁贫硅方向演化)以及钠质拉斑玄武岩系列,均为有利于铁矿化的岩石建造(曾令高等, 2013)。

哈克图解表明,小高山玄武岩和平川铁矿苦橄斑岩均表现出 $Mg^{\#}$ 和 TiO_2、^{T}FeO 的负相关(图 5b 和 5c),以及近平行的稀土元素和微量元素配分模式(图 6),指示了一种连续演化趋势。此外,两者具有

相似的 $\varepsilon Nd(t)$ 值[$\varepsilon Nd(t)_{小高山}=+2.91\sim+3.02$；$\varepsilon Nd(t)_{苦橄斑岩}=+2.3\sim+6.7$，Wang *et al.*, 2014]。这些地球化学特征均表明小高山玄武岩和平川铁矿苦橄斑岩是同源的，并且是连续演化的产物。

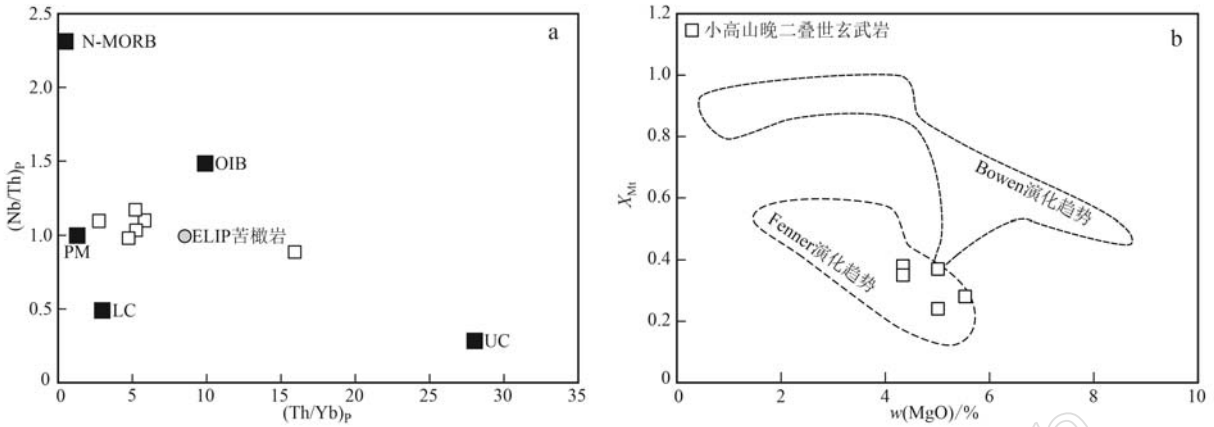

图 8　$(Nb/Th)_P$-$(Th/Yb)_P$ 地壳混染判别图(a，据 Pearce，2008)和 X_{Mt}-$w(MgO)$ 投图(b，据徐义刚等，2003)

Fig. 8　$(Nb/Th)_P$-$(Th/Yb)_P$ plot to discriminate crustal contamination (a, after Pearce, 2008) and plots of X_{Mt}-$w(MgO)$ (b, after Xu Yigang *et al.*, 2003)

数据来源：OIB、原始地幔和大洋中脊玄武岩—Sun and McDonough(1989)；峨眉山苦橄岩—Zhang *et al.*(2006)；扬子上地壳(UC)和下地壳(LC)—Ma *et al.*(2000)和 Wang *et al.*(2007a)

data source: PM, OIB and N-type mid-ocean ridge basalts (N-MORB)—Sun and McDonough (1989); Emeishan picrites—Zhang *et al.* (2006); the Yangtze upper crust (UC) and lower crust (LC)—Ma *et al.* (2000) and Wang *et al.* (2007a)

4.3　源区特征

如前所述，小高山晚二叠世玄武岩的喷发时限为 260.2±5.0 Ma，是峨眉山地幔柱引发的大规模火山作用的同期产物(Zhou *et al.*, 2006; Fan *et al.*, 2008; Zhong *et al.*, 2020; Huang *et al.*, 2022b)。地球化学方面，小高山玄武岩具有亲 OIB 的稀土元素和微量元素配分模式，以及正的 $\varepsilon Nd(t)$ 值(+2.91～+3.02)，均表明起源于地幔柱。Th/Yb-Ta/Yb 投图中，小高山玄武岩投在了 MORB-OIB 阵列之中，介于 E-MORB 和 OIB 之间，且地壳混染不明显(图 9a)。Th/Nb-TiO_2/Yb 地幔柱判别图中(图 9b)，小高山玄武岩投在了 OIB-OPB 范围之内(地幔柱阵列)，并且位于 OIB 与 SZLM 的混合趋势线上(Ⅲb 型；Pearce *et al.*, 2021)，表明地幔源区以地幔柱组分为主，伴有少量的 SZLM 组分。这些判别图显示出和稀土元素微量元素蛛网图以及 Sr-Nd 同位素相似的特征，即小高山晚二叠世玄武岩源区以地幔柱组分为主，并有从 OIB 向 E-MORB 过渡的特征。

4.4　REEBOX 模拟成岩过程

REEBOX PRO(v. 1. 1)模型通过计算地幔熔体的微量元素含量能够对上涌地幔绝热减压熔融过程进行正向模拟。该模型通过实验和热力学约束可定量计算岩石圈底部和最深固相线之间的增量减压过程(0.01×10^3 MPa)中的变压熔融产率(dF/dP)。不同源区岩性单元的瞬时熔体沿着熔融柱发生混合，从而在熔融柱顶部产生一个“熔融柱累积”熔体组分。最后，通过汇集所有“熔融柱累积”熔体计算出大规模岩浆熔融事件的成分。该模型可设定不同源区岩性(比如，橄榄岩、方辉橄榄岩、辉石岩等)、地幔潜温(t_p)以及初始岩石圈厚度(Brown and Lesher, 2016)。根据本文对小高山晚二叠世玄武岩源区特征的约束以及前人研究成果，本文 REEBOX 模型设定的输入参数如下：

采用混合函数“active residual mantle column (RMC, Brown and Lesher, 2016)”，该函数要求源区净浮力值(net source buoyancy)为正值，适用于地幔柱环境(高温地幔柱具有正的净浮力值)。很多研究已证实 ELIP 源区中含有再循环物质(Zhang *et al.*, 2008; Hou *et al.*, 2011; Ren *et al.*, 2017; Zhu *et al.*, 2018; Yang and Liu, 2019; Zhang *et al.*, 2019; Yu *et al.*, 2024)，其中张磊等(2022)对四川盐源平川苦橄岩的研究也表明源区中可能存在辉石岩组分。通过镁同位素研究，Tian 等(2017)进一步指出峨眉山玄武岩源区中再循环组分的比例是较低的。因此，本次模拟将地幔源区岩性及比例设定为：原始地幔(PM, 95%; McDonough and Sun, 1995)代

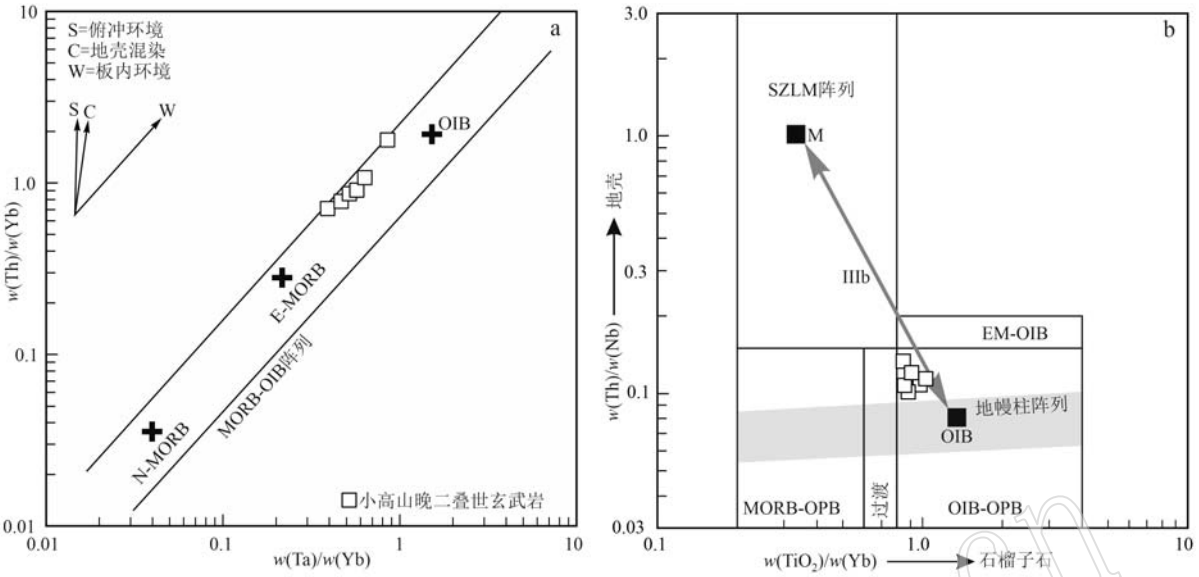

图9 地幔源区判别图 Th/Yb-Ta/Yb 投图(a,据 Pearce,1982)和 Th/Nb-TiO_2/Yb 投图(b,据 Pearce *et al.*,2021)

Fig. 9 Mantle source determination diagrams Th/Yb-Ta/Yb (a, after Pearce, 1982) and Th/Nb-TiO_2/Yb (b, after Pearce *et al.*, 2021)

OPB—大洋高原玄武岩;M—俯冲改造的岩石圈地幔起源的岩浆;EM—富集地幔;OIB—洋岛玄武岩;MORB—大洋中脊玄武岩

OPB—oceanic plateau basalt; M—subduction-modified lithospheric mantle (SZLM) sourced magma; EM— enriched mantle; OIB—ocean island basalts; MORB—mid-ocean ridge basalt

表地幔柱组分(Duncan *et al.*,2016;Heinonen *et al.*,2022);G2 辉石岩(G2 pyroxenite,E-MORB,5%;Sun and McDonough,1989)代表再循环洋壳组分,即辉石岩。前人研究认为峨眉山地幔柱具有异常高温(表7),因此将地幔潜温(t_p)的变化范围设定为1 400~1 690℃,软流圈地幔温度为1 380℃(Heinonen

表7 ELIP 地幔潜温(t_p)、熔融压力以及深度/岩石圈厚度估算结果

Table 7 Estimation of mantle potential temperature (t_p), pressures, and melting depth/lithospheric thickness of the ELIP

地幔潜温(t_p)	熔融压力(p)	熔融深度/岩石圈厚度	参考文献
高钛玄武岩 t_p<1 500℃ 低钛玄武岩 t_p>1 550℃	–	高钛玄武岩初始/终止熔融深度=75~100 km 低钛玄武岩初始/终止熔融深度=60~140 km	Xu *et al.*, 2001
苦橄岩初始源区温度 1 630~1 690℃	4.2×10^3~5.0×10^3 MPa	130~150 km	Zhang *et al.*, 2006; 张招崇等, 2006
苦橄岩 t_p=1 590℃	–	–	Li *et al.*, 2012
峨眉山玄武岩 t_p=1 420~1 637℃	0.4×10^3~4.0×10^3 MPa	地幔源区深度=15~130 km 地壳厚度(终止熔融深度)=64~16 km	李永生, 2012
苦橄质岩浆结晶最大温度=1 440 ℃	–	–	Xu and Liu, 2016
原始岩浆温度>1 600℃	–	原始岩浆熔融深部>130 km	Munteanu *et al.*, 2017
t_p=1 400~1 550℃	2.4×10^3~4.8×10^3 MPa	70~145 km	Shellnutt and Pham, 2018
t_p>1 560℃	~5.0×10^3 MPa	~150 km	Xu *et al.*, 2020
高钛苦橄岩 t_p=1 525~1 620℃ 低-中钛苦橄岩 t_p=1 500~1 550℃;	高钛苦橄岩浆的熔融终止压力: >3×10^3 MPa 低-中钛苦橄岩浆的熔融终止压力:$2\sim3\times10^3$ MPa	高钛苦橄岩浆的熔融终止深度>90 km 低-中钛苦橄岩浆的终止深度= 60~90 km	于宋月等, 2020
高钛熔体 t_p=1 620~1 660℃ 低钛熔体 t_p=1 410~1 530℃	高钛:$4.0\sim5.4\times10^3$ MPa 低钛:$1.5\sim3.0\times10^3$ MPa	高钛=120~160 km 低钛=45~90 km	Yao *et al.*, 2021
t_p=1 450~1 592℃	–	–	Zhang *et al.*, 2021

et al., 2022)。地幔柱与岩石圈强烈相互作用过程中往往伴随着岩石圈的剧烈减薄(Campbell and Griffiths, 1990; Read *et al.*, 2004)。本次工作测定的小高山晚二叠世玄武岩的形成年龄为 260.2±5.0 Ma,与 ELIP 的喷发时限(260~257 Ma),特别是喷发峰期吻合(~260 Ma; 比如 Huang *et al.*, 2022b)。因此,小高山玄武岩形成时期可能发生了大幅度岩石圈减薄。根据学者对 ELIP 熔融深度/岩石圈厚度的估算结果,并考虑估算的不确定性因素(Xu and Liu, 2016; Shellnutt and Pham, 2018),本次模拟设定的岩石圈厚度变化范围是 50~140 km(表 7)。

La/Yb-Ti/Y 投图表明,峨眉山玄武岩投点呈正相关分布,即随着熔融深度增大,Ti/Y 值也随之增大(图10)。这与前人提出的高钛玄武岩形成于较大

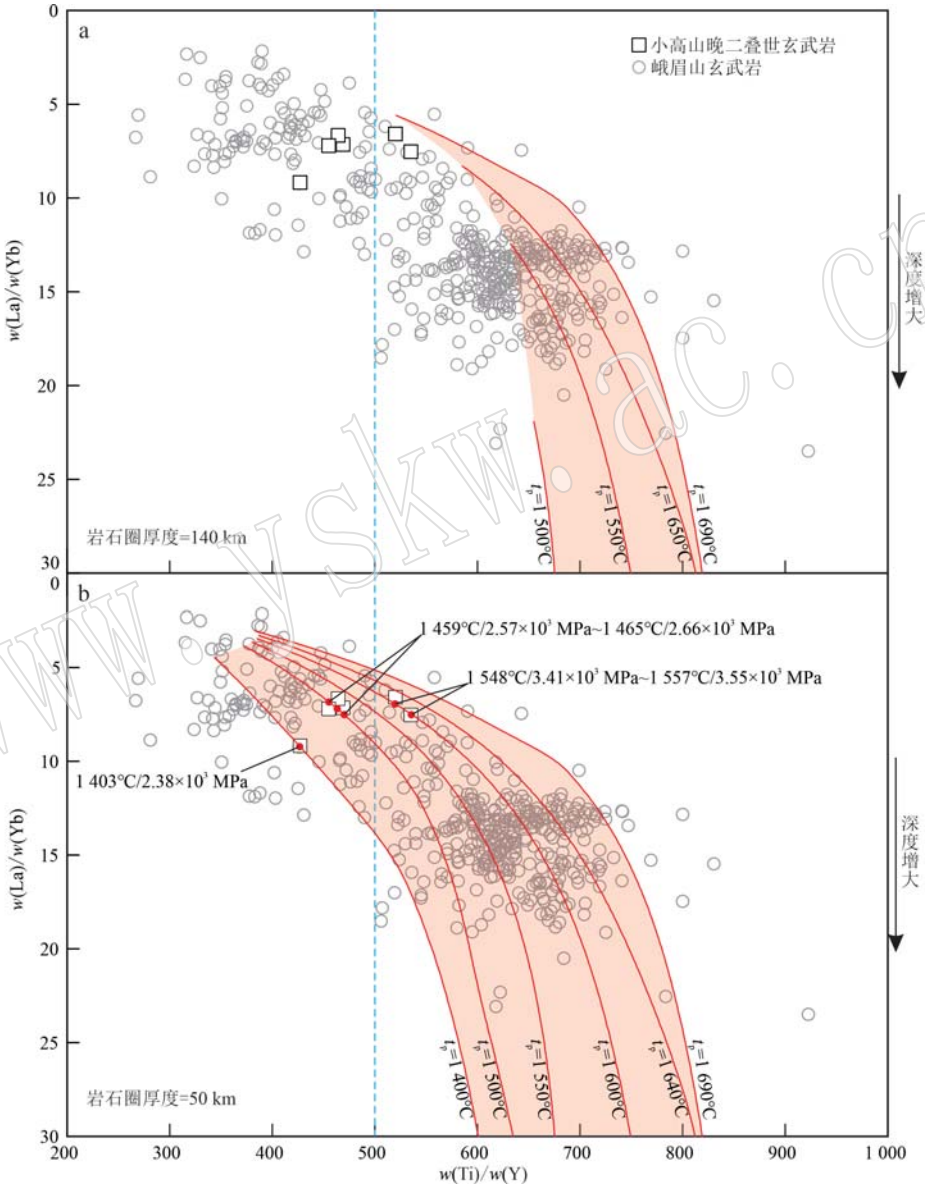

图 10　峨眉山玄武岩的 La/Yb-Ti/Y 投图以及 REEBOX PRO 模拟曲线

Fig. 10　La/Yb-Ti/Y plot and REEBOX PRO modelling for the Emeishan basalts

红色曲线为不同地幔潜温(t_p)条件下的模拟熔融过程,红色圆点代表产生小高山玄武岩的熔融条件。峨眉山玄武岩数据引自:Xu 等(2001); Xiao 等(2003, 2004); Zhou 等(2006); Wang 等(2007a); Song 等(2008); Qi 等(2008); Fan 等(2008); 姜寒冰等(2009); Lai 等(2012); Li 等(2012, 2016, 2017b); Liu 等(2017, 2022); Tian 等(2017); 秦亚等(2018); Yang and Liu(2019); 刘建清等(2020); 戢兴忠等(2021); Yao 等(2021); Huang 等(2022a); Yi 等(2022); 剔除少数异常数据

red curves represent modelling of mantle partial melting at different mantle potential temperatures (t_p), and red dots mark the melting conditions for the Xiaogaoshan basalts. data sources: Emeishan basalts (Xu *et al.*, 2001; Xiao *et al.*, 2003, 2004; Zhou *et al.*, 2006; Wang *et al.*, 2007a; Song *et al.*, 2008; Qi *et al.*, 2008; Fan *et al.*, 2008; Jiang *et al.*, 2009; Lai *et al.*, 2012; Li *et al.*, 2012, 2016, 2017b; Liu *et al.*, 2017, 2022; Tian *et al.*, 2017; Qin *et al.*, 2018; Yang and Liu, 2019; Liu *et al.*, 2020; Ji *et al.*, 2021; Yao *et al.*, 2021; Huang *et al.*, 2022a; Yi *et al.*, 2022; eliminating some outliers)

熔融深度,而低钛玄武岩形成于较浅熔融深度是吻合的(Xu *et al.*, 2001; Xiao *et al.*, 2004; Qi and Zhou, 2008; Fan *et al.*, 2008; Song *et al.*, 2008; Lai *et al.*, 2012; Yao *et al.*, 2021)。峨眉山玄武岩投点呈连续分布,低钛/高钛之间没有明显的间断。

REEBOX PRO 模拟表明,较厚岩石圈条件下(140 km),地幔柱熔融需要较高的 t_p(1 550~1 690℃),模拟熔融曲线覆盖大部分峨眉山高钛玄武岩,但没有延伸到低钛玄武岩区域(图 10a)。因此,较厚岩石圈条件下主要产生高钛玄武岩,这与 Xu 等(2001)的地幔柱熔融模型吻合,同时也符合 ELIP 外带主要是高钛玄武岩的事实(Fan *et al.*, 2008; Lai *et al.*, 2012; Li *et al.*, 2017a)。较薄岩石圈条件下(50 km),不仅熔融的地幔潜温范围变大(t_p=1 400~1 690℃),而且熔融区间也显著扩大。熔融范围既包括了几乎全部的高钛玄武岩,也涵盖相当部分的低钛玄武岩(图 10b)。因此,低钛/高钛玄武岩均可在较薄岩石圈(~50 km)条件下形成,这与 Heinonen 等(2022)对 Karoo LIP 溢流玄武岩的 REEBOX 模拟结果一致。小高山玄武岩可在此条件下形成,其原始岩浆熔融的温压范围是 1 403℃/2.38×10^3 MPa~1 557℃/3.55×10^3 MPa(图 10b)。异常高的熔融温度超出了正常地幔温度~180℃,指示了地幔柱在小高山玄武岩形成过程中的重要作用(Zhang *et al.*, 2006; Bryan and Ernst, 2008)。

因此,峨眉山玄武岩的源区组分以地幔柱组分为主,具有原始地幔特征,并且伴有少量再循环组分(辉石岩,~5%)。Ren 等(2017)通过对 ELIP 苦橄岩橄榄石熔融包裹体的精细研究,提出不同类型的溢流玄武岩(高钛/中钛/低钛)均起源于一个相对均一的源区。Zhang 等(2019)进一步提出了一个连续变压熔融模型,即熔融压力和部分熔融程度是导致不同 Ti 含量以及 Ti/Y 值的关键因素。以上 REEBOX 模拟结果支持了这一论点,即峨眉山低钛/高钛玄武岩可以通过连续熔融形成,决定因素是熔融温度和压力条件以及地幔源区物质组成。

5 结论

(1) 四川盐源小高山晚二叠世玄武岩属于钠质拉斑玄武岩系列。单斜辉石的结晶温度为 1 061~1 180℃,压力为 190~352 MPa。Fe-Ti 氧化物较低的 X_{Mt} 值(0.24~0.38)指示了较低的氧逸度,有利于向 Fenner 趋势演化。

(2) LA-ICP-MS 锆石 U-Pb 测年结果为 260.2±5.0 Ma,小高山玄武岩形成于 ELIP 喷发峰期。玄武岩未遭受明显地壳混染,源区以地幔柱组分为主,与平川铁矿苦橄斑岩具有同源性,是连续分离结晶的产物。

(3) REEBOX PRO 模拟表明,较厚岩石圈(140 km)下需要较高的地幔潜温(t_p = 1 550~1 690℃),且仅能熔出高钛玄武岩。较薄岩石圈(50 km)的熔融范围明显扩大(t_p = 1 400~1 690℃),可熔出高钛和低钛玄武岩。峨眉山低钛/高钛玄武岩是一个具有原始地幔特征的源区经过连续熔融的产物。小高山玄武岩形成于较薄岩石圈条件下,形成的温度压力范围是 1 403℃/2.38×10^3 MPa~1 557℃/3.55×10^3 MPa。

致谢 感谢中国地质博物馆狄友利工程师在野外考察中提供的帮助!

References

Anh T V, Pang K N, Chung S L, *et al*. 2011. The Song Da magmatic suite revisited: A petrologic, geochemical and Sr-Nd isotopic study on picrites, flood basalts and silicic volcanic rocks[J]. Journal of Asian Earth Sciences, 42(6): 1 341~1 355.

Belousova E, Griffin W, O'Reilly S Y, *et al*. 2002. Igneous zircon: Trace element composition as an indicator of source rock type[J]. Contributions to Mineralogy and Petrology, 143(5): 602~622.

Bowen N L. 1928. The Evolution of the Igneous Rocks[M]. Princeton: Princeton University Press.

Brooks C K, Larsen L M and Nielsen T F. 1991. Importance of iron-rich tholeiitic magmas at divergent plate margins: A reappraisal[J]. Geology, 19(3): 269~272.

Brown E L and Lesher C E. 2016. REEBOX PRO: A forward model simulating melting of thermally and lithologically variable upwelling mantle[J]. Geochemistry, Geophysics, Geosystems, 17: 3 929~3 968.

Bryan S E and Ernst R E. 2008. Revised definition of Large Igneous Provinces (LIPs)[J]. Earth-Science Reviews, 86(1~4): 175~202.

Campbell I H and Griffiths R W. 1990. Implications of mantle plume structure for the evolution of flood basalts[J]. Earth and Planetary Science Letters, 99(1~2): 79~93.

Chung S L and Jahn B M. 1995. Plume-lithosphere interaction in generation of the Emeishan flood basalts at the Permian-Trassic boundary [J]. Geology, 23(10): 889~892.

Dong Shuyun and Zhang Zhaochong. 2009. Geochemical behavior of Yttrium in Fe-Ti oxides: An example inferred from the Emeishan Large Igneous Province[J]. Geological Review, 55(3): 355~360 (in Chinese with English abstract).

Duncan R A, Kent A J R, Thornber C R, *et al*. 2016. Timing and composition of continental volcanism at Harrat Hutaymah, western Saudi Arabia[J]. Journal of Volcanology and Geothermal Research, 313: 1~14.

Ewart A, Marsh J S, Milner S C, *et al*. 2004. Petrology and geochemistry of Early Cretaceous bimodal continental flood volcanism of the NW Etendeka, Namibia. Part 1: Introduction, mafic lavas and Re-evaluation of mantle source components[J]. Journal of Petrology, 45(1): 59~105.

Fan W M, Zhang C H, Wang Y J, *et al*. 2008. Geochronology and geochemistry of Permian basalts in western Guangxi Province, Southwest China: Evidence for plume-lithosphere interaction[J]. Lithos, 102(1~2): 218~236.

Fenner C N. 1929. The crystallization of basalt[J]. American Journal of Science, 18: 223~253.

Garapić G, Jackson M G, Hauri E H, *et al*. 2015. A radiogenic isotopic (He-Sr-Nd-Pb-Os) study of lavas from the Pitcairn hotspot: Implications for the origin of EM-1 (enriched mantle 1)[J]. Lithos, 228~229: 1~11.

Guo Mengming. 1990. Regional Survey report of Pingchuan (SHEET G-47-24-B) and Tianwan (SHEET G-47-24-D) with A Scale 1∶50 000: Geological part [R]. 1~110 (in Chinese).

Hanyu T, Kawabata H, Tatsumi Y, *et al*. 2014. Isotope evolution in the HIMU reservoir beneath St. Helena: Implications for the mantle recycling of U and Th[J]. Geochimica et Cosmochimica Acta, 143: 232~252.

Hao Yanli, Zhang Zhaochong, Wang Fusheng, *et al*. 2004. Petrogenesis of high-Ti and low-Ti basalts from the Emeishan Large Igneous Province[J]. Geological Review, 50: 587~592 (in Chinese with English abstract).

He B, Xu Y G, Chung S L, *et al*. 2003. Sedimentary evidence for a rapid, kilometer-scale crustal doming prior to the eruption of the Emeishan flood basalts[J]. Earth and Planetary Science Letters, 213(3~4): 391~405.

He B, Xu Y G, Huang X L, *et al*. 2007. Age and duration of the Emeishan flood volcanism, SW China: Geochemistry and SHRIMP zircon U-Pb dating of silicic ignimbrites, post-volcanic Xuanwei Formation and clay tuff at the Chaotian section[J]. Earth and Planetary Science Letters, 255(3~4): 306~323.

Heinonen J S, Brown E, Turunen S T, *et al*. 2022. Heavy rare earth elements and the sources of continental flood basalts[J]. Journal of Petrology, 63(10): 1~17.

Hill R I. 1991. Starting plumes and continental break-up[J]. Earth and Planetary Science Letters, 104(2~4): 398~416.

Hofmann A W. 1988. Chemical differentiation of the earth: The relationship between mantle, continental crust, and oceanic crust[J]. Earth and Planetary Science Letters, 90(3): 297~314.

Hou T, Zhang Z C, Kusky T, *et al*. 2011. A reappraisal of the high-Ti and low-Ti classification of basalts and petrogenetic linkage between basalts and mafic-ultramafic intrusions in the Emeishan Large Igneous Province, SW China[J]. Ore Geology Reviews, 41(1): 133~143.

Huang H, Cawood P A, Hou M C, *et al*. 2022a. Zircon U-Pb age, trace element, and Hf isotopic constrains on the origin and evolution of the Emeishan Large Igneous Province[J]. Gondwana Research, 105: 535~550.

Huang H, Huyskens M H, Yin Q Z, *et al*. 2022b. Eruptive tempo of Emeishan large igneous province, southwestern China and northern Vietnam: Relations to biotic crises and paleoclimate changes around the Guadalupian-Lopingian boundary[J]. Geology, 50(9): 1 083~1 087.

Hunter R H and Sparks R S J. 1987. The differentiation of the Skaergaard intrusion[J]. Contributions to Mineralogy and Petrology, 95(4): 451~461.

Ji Xingzhong, Chen Qiang, Cheng Zhiguo, *et al*. 2021. Geochronology, geochemistry and petrogenesis of the Pu'an basalt succession from eastern Emeishan large igneous province[J]. Acta Petrologica et Mineralogica, 40(2): 363~383 (in Chinese with English abstract).

Jiang Changyi, Qian Zhuangzhi, Jiang Hanbing, *et al*. 2007. Petrogenesis and source characteristics of low-Ti basalts and picrites at Binchuan-Yongsheng-Lijiang region, Yunnan, China[J]. Acta Petrologica Sinica, 23(4): 777~792 (in Chinese with English abstract).

Jiang Hanbing, Jiang Changyi, Qian Zhuangzhi, *et al*. 2009. Petrogenesis of high-Ti and low-Ti basalts in Emeishan, Yunnan, China[J]. Acta Petrologica Sinica, 25(5): 1 117~1 134 (in Chinese with English abstract).

Jourdan F, Bertrand H, Sharer U, *et al*. 2007. Major-trace element and Sr-Nd-Hf-Pb isotope compositions of the Karoo large igneous province in Botswana-Zimbabwe[J]. Journal of Petrology, 48: 1 043~1 077.

Juster T C, Grove T L and Perfit M R. 1989. Experimental constraints on the generation of FeTi basalts, andesites, and rhyodacites at the Galapagos Spreading Center, 85°W and 95°W[J]. Journal of Geophysical Research: Solid Earth, 94(B7): 9 251~9 274.

Lai S C, Qin J F, Li Y F, *et al*. 2012. Permian high Ti/Y basalts from the eastern part of the Emeishan Large Igneous Province, southwestern China: Petrogenesis and tectonic implications[J]. Journal of Asian Earth Sciences, 47: 216~230.

Lassiter J C, Blichert-Toft J, Hauri E H, *et al*. 2003. Isotope and trace element variations in lavas from Raivavae and Rapa, Cook-Austral islands: Constraints on the nature of HIMU- and EM-mantle and the origin of mid-plate volcanism in French Polynesia[J]. Chemical Geology, 202(1~2): 115~138.

Li C S, Tao Y, Qi L, *et al*. 2012. Controls on PGE fractionation in the Emeishan picrites and basalts: Constraints from integrated lithophile-siderophile elements and Sr-Nd isotopes[J]. Geochimica et Cosmochimica Acta, 90: 12~32.

Li H B, Zhang Z C, Ernst R, *et al*. 2015. Giant radiating mafic dyke swarm of the Emeishan Large Igneous Province: Identifying the mantle plume centre[J]. Terra Nova, 27(4): 247~257.

Li H B, Zhang Z C, Santosh M, *et al*. 2016. Late Permian basalts in the northwestern margin of the Emeishan Large Igneous Province: Implications for the origin of the Songpan-Ganzi terrane[J]. Lithos, 256~257: 75~87.

Li H B, Zhang Z C, Santosh M, *et al*. 2017a. Late Permian basalts in the Yanghe area, eastern Sichuan Province, SW China: Implications for the geodynamics of the Emeishan flood basalt province and Permian global mass extinction[J]. Journal of Asian Earth Sciences, 134: 293~308.

Li J, Zhong H, Zhu W G, *et al*. 2017b. Elemental and Sr-Nd isotopic geochemistry of Permian Emeishan flood basalts in Zhaotong, Yunnan Province, SW China[J]. International Journal of Earth Sciences, 106(2): 617~630.

Li Yongsheng. 2012. Quantitative Modeling of the Emeishan Large Igneous Province Magmatism Processes[D]. Beijing: China University of Geosciences (in Chinese with English abstract).

Liao Baoli, Zhang Zhaochong, Kou Caihua, *et al*. 2012. Geochemistry of the Shuicheng Permian sodium trachybasalts in Guizhou Province and constraints on the mantle sources[J]. Acta Petrologica Sinica, 28(4): 1 238~1 250 (in Chinese with English abstract).

Lightfoot P C, Hawkesworth C J, Hergt J, *et al*. 1993. Remobilisation of the continental lithosphere by a mantle plume: Major-, trace-element, and Sr-, Nd-, and Pb-isotope evidence from picritic and tholeiitic lavas of the Noril'sk District, Siberian Trap, Russia[J]. Contributions to Mineralogy and Petrology, 114(2): 171~188.

Liu Jianqing, He Li, Hu Yuhan, *et al*. 2020. The petrological and geochemical characteristics of Emei Shan basalt in Leibo County, Sichuan Province[J]. Acta Geoscientica Sinica, 41(3): 325~336 (in Chinese with English abstract).

Liu W H, Zhang J, Sun T, *et al*. 2015. Low-Ti iron oxide deposits in the Emeishan large igneous province related to low-Ti basalts and gabbroic intrusions[J]. Ore Geology Reviews, 65: 180~197.

Liu X J, Liang Q D, Li Z L, *et al*. 2017. Origin of Permian extremely high Ti/Y mafic lavas and dykes from Western Guangxi, SW China: Implications for the Emeishan mantle plume magmatism[J]. Journal of Asian Earth Sciences, 141: 97~111.

Liu X Y, Qiu N S, Søager N, *et al*. 2022. Geochemistry of Late Permian basalts from boreholes in the Sichuan Basin, SW China: Implications for an extension of the Emeishan large igneous province[J]. Chemical Geology, 588: 120636.

Luttinen A V. 2018. Bilateral geochemical asymmetry in the Karoo large igneous province[J]. Scientific Reports, 8(1): 5 223.

Ma C Q, Ehlers C, Xu C H, *et al*. 2000. The roots of the Dabieshan ultrahigh-pressure metamorphic terrane: Constraints from geochemistry and Nd-Sr isotope systematics[J]. Precambrian Research, 102(3~4): 279~301.

Madureira P, Mata J, Mattielli N, *et al*. 2011. Mantle source heterogeneity, magma generation and magmatic evolution at Terceira Island (Azores archipelago): Constraints from elemental and isotopic (Sr, Nd, Hf, and Pb) data[J]. Lithos, 126(3~4): 402~418.

Marzoli A, Bertrand H, Youbi N, *et al*. 2019. The Central Atlantic Magmatic Province (CAMP) in Morocco[J]. Journal of Petrology, 60: 945~996.

McDonough W F and Sun S S. 1995. The composition of the Earth[J]. Chemical Geology, 120: 223~253.

Miyashiro A. 1974. Volcanic rock series in island arcs and active continental margins[J]. American Journal of Science, 274(4): 321~355.

Morimoto N, Fabries J, Ferguson A K, *et al*. 1988. Nomenclature of pyroxene[J]. American Mineralogist, 73: 1 123~1 133.

Munteanu M, Wilson A H, Costin G, *et al*. 2017. The mafic-ultramafic dykes in the Yanbian Terrane (Sichuan Province, SW China): Record of magma differentiation and emplacement in the Emeishan Large Igneous Province[J]. Journal of Petrology, 58: 513~538.

Pearce J A. 1982. Trace Element Characteristics of Lavas from Destructive Plateboundaries. Orogenic andesites and Related Rocks[M].

John Wiley and Sons, Chich-ester, England.

Pearce J A. 2008. Geochemical fingerprinting of oceanic basalts with applications to ophiolite classification and the search for Archean oceanic crust[J]. Lithos, 100(1~4): 14~48.

Pearce J A, Ernst R E, Peate D W, *et al*. 2021. LIP printing: Use of immobile element proxies to characterize Large Igneous Provinces in the geologic record[J]. Lithos, 392~393: 106068.

Qi L and Zhou M F. 2008. Platinum-group elemental and Sr-Nd-Os isotopic geochemistry of Permian Emeishan flood basalts in Guizhou Province, SW China[J]. Chemical Geology, 248(1~2): 83~103.

Qin Ya, Yang Qijun, Sun Mingxing, *et al*. 2018. Geological and geochemical characteristics of Hezhang basalt in Guizhou and its response to Emeishan basalt[J]. Journal of Guilin University of Technology, 38(1): 1~13 (in Chinese with English abstract).

Read G, Grutter H, Winter S, *et al*. 2004. Stratigraphic relations, kimberlite emplacement and lithospheric thermal evolution, Quiricó Basin, Minas Gerais State, Brazil[J]. Lithos, 77(1~4): 803~818.

Regional Geological Survey Team No. 1, Sichuan Geologic Bureau. 1971. Geological survey report of Yanyuan (SHEET G-47-6) with a scale of 1:200,000 [R]: 1~75 (in Chinese).

Ren Z Y, Wu Y D, Zhang L, *et al*. 2017. Primary magmas and mantle sources of Emeishan basalts constrained from major element, trace element and Pb isotope compositions of olivine-hosted melt inclusions [J]. Geochimica et Cosmochimica Acta, 208: 63~85.

Saunders A D. 2005. Large igneous provinces: Origin and environmental consequences[J]. Elements, 1(5): 259~263.

Shellnutt J G and Jahn B M. 2011. Origin of Late Permian Emeishan basaltic rocks from the Panxi region (SW China): Implications for the Ti-classification and spatial-compositional distribution of the Emeishan flood basalts[J]. Journal of Volcanology and Geothermal Research, 199(1~2): 85~95.

Shellnutt J G and Pham T T. 2018. Mantle potential temperature estimates and primary melt compositions of the Low-Ti Emeishan flood basalt[J]. Frontiers in Earth Science, 6: 67.

Smith J V and Brown W L. 1974. Feldspar Minerals[M]. Springer-Verlag, Germany.

Song Biao, Zhang Yuhai, Wan Yusheng, *et al*. 2002. Mount making and procedure of the SHRIMP Dating [J]. Geological Review, 48 (sup.): 26~30 (in Chinese with English abstract).

Song X Y, Qi H W, Robinson P T, *et al*. 2008. Melting of the subcontinental lithospheric mantle by the Emeishan mantle plume; evidence from the basal alkaline basalts in Dongchuan, Yunnan, Southwestern China[J]. Lithos, 100(1~4): 93~111.

Sun S S and McDonough W F. 1989. Chemical and isotopic systematics of oceanic basalt: Implications for mantle composition and processes [J]. Geological Society, London, Special Publication, 42(1): 313~345.

Sun Y D, Lai X L, Wignall P B, *et al*. 2010. Dating the onset and nature of the Middle Permian Emeishan large igneous province eruptions in SW China using conodont biostratigraphy and its bearing on mantle plume uplift models[J]. Lithos, 119(1~2): 20~33.

Tegner C, Lesher C E, Larsen L M, *et al*. 1998. Evidence from the rare-earth-element record of mantle melting for cooling of the Tertiary Iceland plume[J]. Nature, 395: 591~594.

Tian H C, Yang W, Li S G, *et al*. 2017. Could sedimentary carbonates be recycled into the lower mantle? Constraints from Mg isotopic composition of Emeishan basalts[J]. Lithos, 292~293: 250~261.

Toplis M J and Carroll M R. 1995. An experimental study of the influence of oxygen fugacity on Fe-Ti oxide stability, phase relations and mineral-melt equilibria in ferro-basaltic systems[J]. Journal of Petrology, 36: 1 137~1 170.

Veklser I V. 2009. Extreme iron enrichment and liquid immiscibility in mafic intrusions: Experimental evidence revisited[J]. Lithos, 111(1~2): 72~82.

Wang C Y, Zhou M F and Qi L. 2007a. Permian flood basalts and mafic intrusions in the Jinping (SW China)-Song Da (northern Vietnam) district: Mantle sources, crustal contamination and sulfide segregation[J]. Chemical Geology, 243: 317~343.

Wang M, Zhang Z C, Santosh M, *et al*. 2014. Geochemistry of Late Permian picritic porphyries and associated Pingchuan iron ores, Emeishan Large Igneous Province, Southwest China: Constraints on petrogenesis and iron sources[J]. Ore Geology Reviews, 57: 602~617.

Wang X D, Hou T, Wang M, *et al*. 2021. A new clinopyroxene thermobarometer for mafic to intermediate magmatic systems[J]. European Journal of Mineralogy, 33(5): 621~637.

Wang Y, Yang J D, Chen J, *et al*. 2007b. The Sr and Nd isotopic variations of the Chinese Loess Plateau during the past 7 Ma: Implications for the East Asian winter monsoon and source areas of Loess[J]. Palaeogeography, Palaeoclimatology, Palaeoecology, 249(3~4): 351~361.

Wang Yan, Wang Kun, Xing Changming, *et al*. 2017. Metallogenic diversity related to the late middle Permian Emeishan Large Igneous Province[J]. Bulletin of Mineralogy, Petrology and Geochemistry, 36(3): 404~417 (in Chinese with English abstract).

Wang Yunfeng, Zhang Zhaochong, Wang Lijuan, *et al*. 2013. Geochemical characteristics of Permian basalt from Hutiaoxia and Jin'an area of

the Emeishan Large Igneous Province and constraints on their source region[J]. Acta Petrologica Sinica, 29(12): 4 387~4 403 (in Chinese with English abstract).

Xiao L, Xu Y G, Chung S L, *et al*. 2003. Chemostratigraphic correlation of upper Permian lava succession from Yunnan province, China: Extent of the Emeishan large igneous province[J]. International Geology Review, 45: 753~766.

Xiao L, Xu Y G, Mei H J, *et al*. 2004. Distinct mantle sources of low-Ti and high-Ti basalts from the western Emeishan large igneous province, SW China: Implications for plume-lithosphere interaction[J]. Earth and Planetary Science Letters, 228(3~4): 525~546.

Xu J F, Suzuki K, Xu Y G, *et al*. 2007. Os, Pb, and Nd isotope geochemistry of the Permian Emeishan continental flood basalts: Insights into the source of a large igneous province[J]. Geochimica et Cosmochimica Acta, 71(8): 2 104~2 119.

Xu R and Liu Y S. 2016. Al-in-olivine thermometry evidence for the mantle plume origin of the Emeishan large igneous province[J]. Lithos, 266~267: 362~366.

Xu R, Liu Y S and Lambart S. 2020. Melting of a hydrous peridotite mantle source under the Emeishan large igneous province[J]. Earth-Science Reviews, 207: 103253.

Xu Y G, Chung S L, Jahn B M, *et al*. 2001. Petrologic and geochemical constraints on the petrogenesis of Permian-Triassic Emeishan flood basalts in southwestern China[J]. Lithos, 58(3~4): 145~168.

Xu Yigang, Mei Houjun, Xu Jifeng, *et al*. 2003. Origin of two differentiation trends in the Emeishan flood basalts. Chinese Science Bulletin, 48(4): 383~387 (in Chinese with English abstract).

Yang C and Liu S A. 2019. Zinc isotope constraints on recycled oceanic crust in the mantle sources of the Emeishan Large Igneous Province [J]. Journal of Geophysical Research: Solid Earth, 124(12): 12 537~12 555.

Yao J H, Zhu W G, Wang Y J, *et al*. 2021. Geochemistry of the Yumen picrites-basalts from the Emeishan large igneous province: Implications for their mantle source, PGE behaviors, and petrogenesis[J]. Lithos, 400~401: 106364.

Yi D, Zhao J, Li C H, *et al*. 2022. Crustal contaminations responsible for the petrogenesis of basalts from the Emeishan Large Igneous Province, NW China: New evidence from Ba isotopes[J]. Journal of Earth Science, 33(1): 109~120.

Yu S Y, Song X Y and Chen L M. 2024. Interaction between mantle plume and subduction-modified lithospheric mantle: Geochemical evidence from the picritic lavas from the Emeishan large igneous province[J]. Chemical Geology, 648: 121964.

Yu Songyue, Lan Jiangbo, Chen Qi. 2020. The compositional inversion and evaluation of melting conditions for primary melt of the Emeishan picrites[J]. Bulletin of Mineralogy, Petrology and Geochemistry, 39(6): 1 240~1 255 (in Chinese with English abstract).

Zeng Linggao, Zhang Jun, Sun Teng, *et al*. 2013. Zircon U-Pb age of mafic-ultramafic rock from Pingchuan region in Southern Sichuan and its geological implications[J]. Earth Science-Journal of China University of Geosciences, 38(6): 1 197~1 213 (in Chinese with English abstract).

Zhang L, Ren Z Y, Handler M R, *et al*. 2019. The origins of high-Ti and low-Ti magmas in large igneous provinces, insights from melt inclusion trace elements and Sr-Pb isotopes in the Emeishan large Igneous Province[J]. Lithos, 344~345: 122~133.

Zhang L, Ren Z Y, Zhang L, *et al*. 2021. Nature of the mantle plume under the Emeishan large igneous province: Constraints from olivine-hosted melt inclusions of the Lijiang picrites[J]. Journal of Geophysical Research: Solid Earth, 126(5): e2020JB021022.

Zhang Lei, Ren Zhongyuan and Zhang Le. 2022. The nature of mantle source of the Pingchuan picrites in the Emeishan Large Igneous Province: Constrains from the trace element composition of olivines [J]. Geotectonica et Metallogenia, 46(1): 112~131 (in Chinese with English abstract).

Zhang Zhaochong. 2009. A discussion on some important problems concerning the Emeishan large igneous province[J]. Geology in China, 36(3): 634~646 (in Chinese with English abstract).

Zhang Z C, Kang J L, Kusky T, *et al*. 2012. Geochronology, geochemistry and petrogenesis of Neoproterozoic basalts from Sugetbrak, northwest Tarim block, China: Implications for the onset of Rodinia supercontinent breakup[J]. Precambrian Research, 220~221: 158~176.

Zhang Z C, Mahoney J J, Mao J W, *et al*. 2006. Geochemistry of picritic and associated basalt flows of the western Emeishan flood basalt province, China[J]. Journal of Petrology, 47(10): 1 997~2 019.

Zhang Z C, Mao J W, Saunders A D, *et al*. 2009. Petrogenetic modeling of three mafic-ultramafic layered intrusions in the Emeishan large igneous province, SW China, based on isotopic and bulk chemical constraints[J]. Lithos, 113(3~4): 369~392.

Zhang Z C, Zhi X C, Chen L, *et al*. 2008. Re-Os isotopic compositions of picrites from the Emeishan flood basalt province, China[J]. Earth and Planetary Science Letters, 276(1~2): 30~39.

Zhang Zhaochong, Mahoney John J, Wang Fusheng, *et al*. 2006. Geochemistry of picritic and associated basalt flows of the western Emeishan flood basalt province, China: Evidence for a plume-head origin

[J]. Acta Petrologica Sinica, 22(6): 1 538~1 552 (in Chinese with English abstract).

Zhang Zhaochong, Wang Fusheng, Fan Weiming, *et al*. 2001. A discussion on some problems concerning the study of the Emeishan basalts [J]. Acta Petrologica et Mineralogica, 20(3): 239~246 (in Chinese with English abstract).

Zhong Y T, Mundil R, Chen J, *et al*. 2020. Geochemical, biostratigraphic, and high-resolution geochronological constraints on the waning stage of Emeishan Large Igneous Province[J]. Geological Society of America Bulletin, 132(9~10): 1 969~1 986.

Zhou M F, Zhao J H, Qi L, *et al*. 2006. Zircon U-Pb geochronology and elemental and Sr-Nd isotope geochemistry of Permian mafic rocks in the Funing area, SW China[J]. Contributions to Mineralogy and Petrology, 151(1): 1~19.

Zhu J, Zhang Z C, Reichow M K, *et al*. 2018. Weak vertical surface movement caused by the ascent of the Emeishan mantle anomaly[J]. Journal of Geophysical Research: Solid Earth, 123(2): 1 018~1 034.

附中文参考文献

董书云, 张招崇. 2009. 钇(Y)在铁钛氧化物中的地球化学行为——以峨眉山大火成岩省为例[J]. 地质论评, 55(3): 355~360.

郭孟明. 1990. 平川幅(G-47-24-B)田湾幅(G-47-24-D)1∶5 万区域地质调查报告: 地质部分[R]. 1~110.

郝艳丽, 张招崇, 王福生, 等. 2004. 峨眉山大火成岩省"高钛玄武岩"和"低钛玄武岩"成因探讨[J]. 地质论评, 50(6): 587~592.

戢兴忠, 陈　强, 程志国, 等. 2021. 峨眉山大火成岩省东区普安玄武岩系年代学、地球化学及成因研究[J]. 岩石矿物学杂志, 40(2): 363~382.

姜常义, 钱壮志, 姜寒冰, 等. 2007. 云南宾川-永胜-丽江地区低钛玄武岩和苦橄岩的岩石成因与源区性质[J]. 岩石学报, 23(4): 777~792.

姜寒冰, 姜常义, 钱壮志, 等. 2009. 云南峨眉山高钛和低钛玄武岩的岩石成因[J]. 岩石学报, 25(5): 1 117~1 134.

李永生. 2012. 峨眉山大火成岩省岩浆作用过程的定量模拟[D]. 北京: 中国地质大学(北京).

廖宝丽, 张招崇, 寇彩化, 等. 2012. 贵州水城二叠纪钠质粗面玄武岩的地球化学特征及其源区[J]. 岩石学报, 28(4): 1 238~1 250.

刘建清, 何　利, 胡宇瀚, 等. 2020. 四川雷波峨眉山玄武岩岩石学及地球化学特征[J]. 地球学报, 41(3): 325~336.

秦　亚, 杨启军, 孙明行, 等. 2018. 贵州赫章地区玄武岩地质地球化学特征及其对峨眉山玄武岩的响应[J]. 桂林理工大学学报, 38(1): 1~13.

四川地质局第 1 区测队. 1971. 盐源幅 1∶20 万(G-47-6)区域地质测量报告[R]. 1~75.

宋　彪, 张玉海, 万渝生, 等. 2002. 锆石 SHRIMP 样品靶制作、年龄测定及有关现象讨论[J]. 地质论评, 48(S1): 26~30.

王　焰, 王　坤, 邢长明, 等. 2017. 二叠纪峨眉山地幔柱岩浆成矿作用的多样性[J]. 矿物岩石地球化学通报, 36(3): 404~417.

汪云峰, 张招崇, 王丽娟, 等. 2013. 峨眉山大火成岩省虎跳峡和金安二叠纪玄武岩的地球化学特征及其对源区的约束[J]. 岩石学报, 29(12): 4 387~4 403.

徐义刚, 梅厚钧, 许继峰, 等. 2003. 峨眉山大火成岩省中两类岩浆分异趋势及其成因[J]. 科学通报, 48(4): 383~387.

于宋月, 蓝江波, 陈　琦. 2020. 峨眉山苦橄岩原始岩浆成分反演及对地幔熔融条件的评估[J]. 矿物岩石地球化学通报, 39(6): 1 240~1 255.

曾令高, 张　均, 孙　腾, 等. 2013. 川南平川镁铁质-超镁铁质岩锆石 U-Pb 年龄及地质意义[J]. 地球科学—中国地质大学学报, 38(6): 1 197~1 213.

张　磊, 任钟元, 张　乐. 2022. 峨眉山大火成岩省平川苦橄岩地幔源区性质——来自橄榄石微量元素的制约[J]. 大地构造与成矿学, 46(1): 112~131.

张招崇. 2009. 关于峨眉山大火成岩省一些重要问题的讨论[J]. 中国地质, 36(3): 634~646.

张招崇, Mahoney John J, 王福生, 等. 2006. 峨眉山大火成岩省西部苦橄岩及其共生玄武岩的地球化学: 地幔柱头部熔融的证据[J]. 岩石学报, 22(6): 1 538~1 552.

张招崇, 王福生, 范蔚茗, 等. 2001. 峨眉山玄武岩研究中的一些问题的讨论[J]. 岩石矿物学杂志, 20(3): 239~246.